RESEARCH



In situ monitoring of mitochondrial redox dynamics during cardiac reprogramming using a poly-L-lysine/Matrigel-coated gold nanostructured composite platform

Kyeong-Mo Koo¹ · Seung Ju Seo² · Chang-Dae Kim¹ · Hyeon Yang² · Yoonhee Jin² · Tae-Hyung Kim¹,³

Received: 1 February 2025 / Revised: 28 April 2025 / Accepted: 9 May 2025 © The Author(s) 2025

Abstract

Cardiac regeneration via the direct reprogramming of fibroblasts into chemically induced cardiomyocyte-like cells (CiCMs) offers a potential therapeutic avenue for heart failure. Nonetheless, the absence of non-invasive techniques for evaluating CiCM maturation and functionality while maintaining therapeutic viability poses a considerable challenge. We present poly-L-lysine, and Matrigel double layer—coated gold nanostructured (PMGN) composite platform coupled with an electrochemical (EC) method that effectively monitors mitochondrial redox dynamics in CiCMs. Based on the metabolic transition from glycolysis to oxidative phosphorylation (OXPHOS), this EC method provides precise measurement of fibroblast-to-CiCM conversion in a completely non-destructive manner. Moreover, the PMGN composite platform facilitates the early detection of functional alterations induced by drugs, such as isoproterenol and carbachol, which conventional cell viability assays fail to detect, and exhibits exceptional sensitivity in identifying drug-induced cardiotoxicity. This in situ method offers real-time feedback and rapid quality control during cell preparation, significantly enhancing the safety and efficacy of stem-cell-based therapies for cardiac regeneration.

Keywords Cell adhesion polymers · Gold nanostructures · Electrochemical method · Direct cardiac reprogramming · Mitochondrial metabolism · Cardiotoxicity testing

1 Introduction

Heart disease remains the leading cause of death worldwide. The limited regenerative capacity of adult heart presents considerable challenges in recovering from heart failure [1,

Kyeong-Mo Koo and Seung Ju Seo contributed equally to this work.

- ☐ Tae-Hyung Kim thkim0512@skku.edu

Published online: 30 May 2025

- Department of Intelligent Precision Healthcare Convergence, Institute for Cross-Disciplinary Studies (ICS), Sungkyunkwan University (SKKU), Suwon, Gyeonggi 16419, Republic of Korea
- Department of Physiology, Graduate School of Medical Science, Brain Korea 21 Project, Yonsei University College of Medicine, Seoul 03722, Republic of Korea
- Department of Biomedical Engineering, ICS, SKKU, Suwon, Gyeonggi 16419, Republic of Korea

2]. Current pharmacological and surgical treatments primarily focus on alleviating symptoms and decelerating disease progression, rather than restoring myocardial function [3]. Consequently, developing cardiac regeneration strategies is of paramount importance. Direct reprogramming, which transforms somatic cells into different cell types without a pluripotent intermediate, offers a promising approach [4–6]. Notably, direct chemical reprogramming using small-molecule compounds reduces risks associated with teratoma formation and immunogenicity issues compared to gene transfection methods that use transcription factors or microRNAs [7–9]. In this context, chemically induced cardiomyocytelike cells (CiCMs) derived from fibroblasts through small molecules emerge as a safe and effective source of functional cardiomyocytes, offering substantial promise for enhancing cardiac regeneration therapies [10–12].

To confirm the therapeutic viability of CiCMs, comprehensive biological analyses are necessary to assess their maturation and functionality [13–15]. Techniques commonly used include cell viability assays, quantitative polymerase chain reaction (qPCR), immunocytochemical



staining, calcium imaging, and mitochondrial metabolism analysis [16–19]. However, these conventional tools are often labor-intensive, time-consuming, and invasive, necessitating the destruction of cells, which limits assessments of cells targeted for transplantation. FDA guidelines for stem cell quality control mandate assessments such as sterility, viability, genetic stability, and functionality, which compound these challenges [20–22]. These limitations impede efficient evaluation of cell functionality and pose significant challenges to the clinical application of CiCMs, where real-time quality control and functional validation are crucial.

Previously, we developed a novel electrochemical (EC) approach that demonstrated redox signals in living cells primarily result from metabolic processes, particularly the electron transport chains during oxidative phosphorylation (OXPHOS) [23, 24]. Given the metabolic shift from glycolysis to OXPHOS during the direct reprogramming of fibroblasts to CiCMs [25–28], we hypothesized that this transition could be effectively monitored using the EC method in a completely non-invasive way. As CiCMs mature, they increasingly depend on OXPHOS for the significant energy required for contraction [29-31], which is reflected in the EC signal intensity. However, due to the hydrophilic nature of the gold nanostructure film essential for EC detection, Matrigel (Mat), a key component for CiCM culture, could not be adequately coated. High Mat film stability is crucial for effective fibroblast conversion and the acquisition of reliable, adhesion-dependent EC signals. To resolve this, poly-L-lysine (PLL), a cationic polymer, was introduced as an interfacial layer to improve Mat film coating on the electrode through strong interactions with the negatively charged extracellular matrix (ECM) components in Mat. The poly-L-lysine and Matrigel double layer-coated gold nanostructured composites, referred to as PMGN in this study, facilitates non-destructive and rapid (less than 30 s) monitoring of dynamic changes during direct cardiac reprogramming, effectively surpassing the limitations of conventional methods (Fig. 1a). Utilizing the PMGN composites with EC detection, cardiac functions were monitored for extended periods up to 29 days (Fig. 1b) following exposure to isoproterenol (ISO) and carbachol (Cch). The toxicity of several cardiotoxic candidates (doxorubicin, remdesivir, and rosiglitazone) along with a non-toxic drug (liraglutide) was further assessed based on EC signal intensities. In contrast to conventional methods, the PMGN platform does not negatively affect cardiac function or cell viability, thereby permitting the reuse of cells for subsequent analyses. This characteristic allows for more effective assessments of CiCMs for immediate use in cell therapy, thus facilitating clinical applications (Fig. 1c).



2 Materials and methods

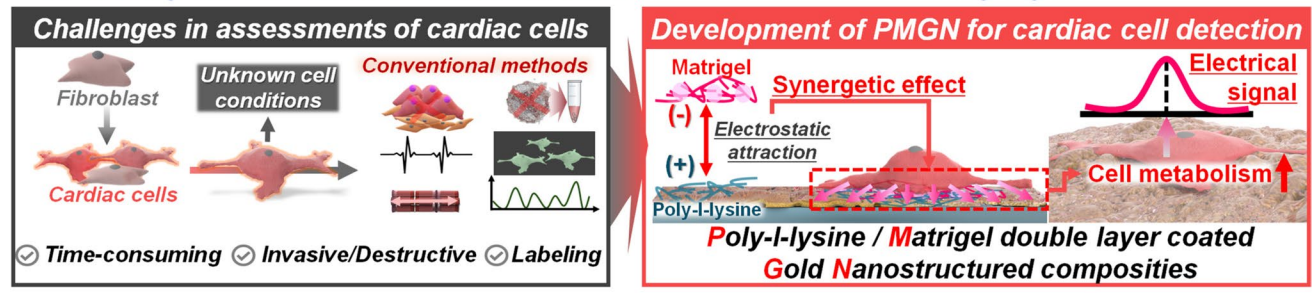
2.1 Isolation and cultivation of primary mouse embryonic fibroblasts

The Institutional Animal Care and Use Committee (IACUC) of Yonsei University Health System granted approval for the isolation of primary mouse embryonic fibroblasts (pMEFs) under permit number 2033-0055. pMEFs were isolated from 13.5-day embryos of ICR mice (Orientbio, Seongnam, South Korea) following previously reported methods [10, 32]. Briefly, the heads, tails, limbs, internal organs, and vertebral columns of the embryos were removed, and the remaining tissues were finely minced. Subsequently, the minced tissue was thoroughly washed with Dulbecco's phosphate-buffered saline (DPBS; Sigma-Aldrich, St. Louis, MO, USA) before being seeded in T75 flasks coated with 0.2% (w/v) gelatin (Sigma-Aldrich), containing pMEF medium (Dulbecco's Modified Eagle Medium (DMEM; #11995065, Thermo Fisher Scientific, Waltham, MA, USA), 10% (v/v) fetal bovine serum (FBS; Thermo Fisher Scientific), 1% (v/v) penicillin-streptomycin (Thermo Fisher Scientific), and 1% (v/v) nonessential amino acids (NEAA; Thermo Fisher Scientific)). The pMEFs were maintained at 37 °C in a 5% CO₂ incubator, and the medium was replaced the following day.

2.2 Fabrication of PLL and Mat-coated gold nanostructure (PMGN) composites

To construct the PMGN platform, materials such as ITO glass, gold chloride trihydrate (AuCl₃), poly(ethylene glycol) 200 (PEG 200), Triton X-100 (Sigma-Aldrich), DPBS (Sigma-Aldrich, St. Louis, MO, USA), polydimethylsiloxane (PDMS), and plastic chambers were sourced from U.I.D (Cheongju, South Korea), Sigma-Aldrich (St. Louis, MO, USA), and Dow Corning Corp. (Midland, MI, USA), respectively. Solutions used in this study were prepared using deionized (DI) water, purified by a Millipore Milli-Q Direct Water Purification System (EMD Millipore, MA, USA). The construction of a highly conductive gold nanostructure (HCGN) on the ITO substrate (total area $1.2 \text{ cm} \times 1.7 \text{ cm}$; thickness 0.07 cm; electrical resistance 9 ohms) utilized a multi-step potential (MSP) channel on the EC instrument for 120 s, as previously described. To prevent structural defects in the gold nanostructure, the ITO-coated glass was sequentially washed with a solution of 1% Triton X-100 in distilled water and 70% ethanol using an ultrasonic cleaner. A plastic chamber measuring 1.7 cm in diameter was attached to the sterilized ITO substrate using PDMS (10:1) as a biocompatible adhesive,

a Necessity for non-invasive and real-time assessments of cardiomyocytes



b Maturation assessments of direct cardiac reprogramming in real-time



c Application for cardiac cell function and cardiotoxicity testing using PMGN platform

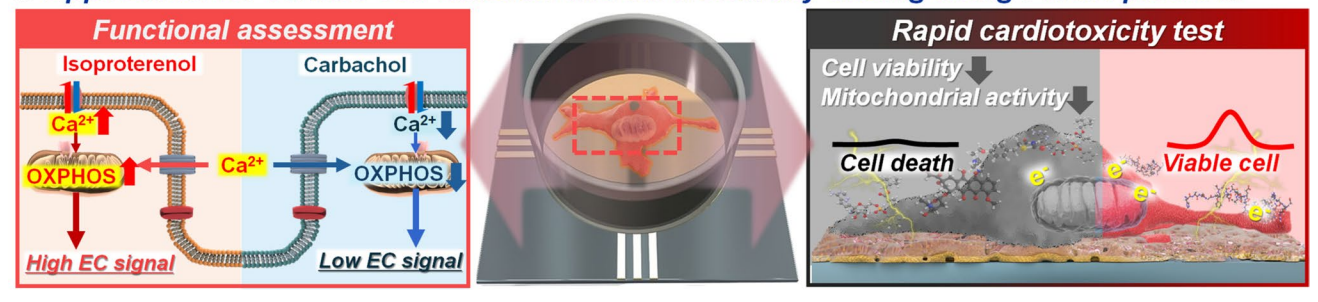


Fig. 1 Schematic illustration of in situ monitoring for direct cardiac reprogramming and its applications using the PMGN composite platform

facilitating the ED process of the gold mixture solution and supporting cellular growth on a chip. A freshly prepared solution containing 5 mM gold (III) chloride and polyethylene glycol (PEG) at a 50:1 ratio was used. The ED of the gold mixture solution (5 mM HAuCl₄) was carried out using the MSP method for 180 s, as previously reported. Subsequently, thermal annealing was applied to the prepared gold nanostructures at 100 °C for 10 min. The completed cell chips were then washed with 70% ethanol and sterilized under UV light for 40 min. Following sterilization, the gold nanostructured platform was initially coated with 200 µg/mL PLL and incubated at 37 °C for 1 h, followed by three washes with distilled water. The PLL-coated gold nanostructured composites were subsequently layered with Matrigel (#354234, Corning Incorporated, Corning, NY, USA) diluted 1:50 and maintained at 37 °C for at least 1 h to support the cultivation of CiCMs.

2.3 Topological and morphological characterization of the PMGN composites

To characterize the surface of the PMGN composites, we utilized FE-SEM (Carl Zeiss, Germany), AFM (Park Systems, South Korea), and c-AFM (XE-100, Park Systems, South Korea). FE-SEM was conducted at an acceleration voltage of 10 kV, whereas AFM was employed in tapping mode (PR-T300, Probes, South Korea). For c-AFM analysis, a platinum-coated tip was used to apply an electrical potential between the tip and the PMGN platform's bottom. The sample bias voltage was set at 5 V. For determining the size of the gold nanoparticles and calculating the root mean square of roughness ($R_{\rm q}$) for each sample, the image processing and analytical program XEI was used. This software enabled us to calculate both the total area of roughness and conductivity of the PMGN composites.



2.4 Visualization of morphological changes in CiCMs on the PMGN composites

To assess the morphology of the CiCMs (day 22) on different groups (no coating; control, and PMGN platform), we fixed the CiCMs with a 10% neutral-buffered formalin (NBF) solution for 15 min, followed by rinsing with DPBS twice. After the washing steps, the CiCMs were dehydrated using a series of ethanol solutions at concentrations of 50%, 60%, 70%, 80%, 90%, and 100% or hexamethyldisilazane (HMDS) for 15 to 20 min. The dehydrated cardiomyocytes were then visualized using FE-SEM.

2.5 EC Detection of direct cardiac reprogramming

The cyclic voltammetry (CV) and differential pulse voltammetry (DPV) experiments were conducted using a DY2013

Potentiostat (EG Technology, Seoul, South Korea). The fabricated PLL/Mat gold nanostructure/ITO electrode acted as the working electrode, with platinum and Ag/AgCl (1 M KCl) wires serving as the counter and reference electrodes, respectively. Prior to the EC detection, the culture medium was replaced with fresh medium to eliminate potential signal interference from redox molecules and metabolites during the direct cardiac reprogramming over 29 days. CV method conditions were set as follows: initial E(V) = 0, high E(V)= 0.3, low E (V) = -0.3, and scan rate (V) = 0.05. For precise quantification, DPV signals were measured under these conditions: initial E (V) = -0.3, final E (V) = 0.4, step E (V) = 0.005, and pulse period (s) = 0.2. Both CV and DPV measurements were performed at RT. The calculated I_p values were analyzed by subtracting the baseline current from the current at $E_p = -0.03$ V. The limit of quantification (LOQ) from the DPV signals was determined using the following formula:

Limits of quantification (LOQ) = $\frac{10\sigma}{S}(\sigma : standard error, S : slope)$

Following the DPV detection, the CiCMs on the PMGN platform were detached using a 0.05% Trypsin–EDTA solution (Thermo Fisher Scientific), and the final cell count was conducted using the SOL COUNT automatic cell counter (SOL Inc., South Korea).

For precise calculation of the active surface area of the PMGN platform, the Randles–Sevcik equation was used, described as follows.

$$i_p = (2.69 \times 10^5) n^{3/2} A D^{1/2} v^{1/2} C$$

where i_p = peak current, n = number of electrons involved, A = electrode area in m^2 , D = diffusion coefficient in m^2 /s, v = scan rate in V/s, and C = concentrations of analytes in mol/L.

2.6 Chemical induction of pMEFs into CiCMs on tissue culture plate and PMGN platform

For cardiac reprogramming on tissue culture plate (TCP) and PMGN surfaces, PMGN were initially coated with 200 μ g/mL PLL and Mat diluted 1:50 (v/v) in DMEM/F12 and incubated at 37 °C for at least 1 h prior to cell seeding. In contrast, TCP plates were coated solely with Mat, without any prior PLL coating. pMEFs were seeded at a density of 2.5×10^4 cells/mL onto coated PMGN and TCP plates. Four hours after seeding, the pMEF medium was replaced with CiCM medium to initiate cardiac reprogramming. CiCM medium consisted of DMEM/F12, 15% (v/v) FBS, 5% (v/v) knockout serum replacement (KSR; Thermo Fisher Scientific), 1% (v/v) penicillin–streptomycin, 1% (v/v) NEAA,

1% (v/v) GlutaMax (Thermo Fisher Scientific), 0.1 mM β- mercaptoethanol, and four small molecules (15 μM Forskolin (#F-9929, LC Laboratory), 10 μM CHIR99021 (#C-6556, LC Laboratory, Woburn, MA, USA), 2 μM A83-01 (#2939, Tocris Bioscience, Bristol, UK), and 1 μM SC-1 (#10009557, Cayman Chemical, Ann Arbor, MI, USA)) [10, 11]. The CiCM medium was maintained at 37°C with 5% CO_2 , with changes made every other day.

2.7 Immunocytochemical staining

After washing with PBS, the cells were fixed with a 10% (v/v) formalin solution (Sigma-Aldrich) for 10 min at RT. They were then permeabilized with 0.1% (v/v) Triton X-100 for 10 min at RT. Subsequently, the cells were blocked with 5% (w/v) bovine serum albumin (BSA; 0216006980, MP Biomedicals, Irvine, CA, USA) for 1 h at RT. Next, the cells were incubated overnight with primary antibodies at 4 °C. The primary antibodies used in this study were mouse antiα-actinin (1:500; A7811, Sigma-Aldrich), mouse anti-cardiac Troponin T (cTnT; 1:200; MA5-12960, Thermo Fisher Scientific), and mouse anti-Gata4 (1:200; sc-25310, Santa Cruz Biotechnology, Dallas, TX, USA). After thorough washing with PBS three times, the cells were incubated with secondary antibodies for 1 h at RT. The secondary antibodies used in this study were Alexa-Fluor 488 goat anti-mouse IgG (1:200; A11001, Thermo Fisher Scientific) and Alexa-Fluor 594 goat anti-mouse IgG (1:200; A11005, Thermo Fisher Scientific). The F-actin cytoskeleton was stained with Phalloidin-iFluor 594 Reagent (1:1000; ab176757, Abcam,



Cambridge, UK) for 1 h at 4 °C. To visualize t-tubules, FITC-conjugated wheat germ agglutinin (WGA; 5 µg/ml; L4895, Sigma-Aldrich) was used, which binds to N-acetyl-D-glucosamine and sialic acid. After secondary antibody staining, the cells were washed three times or more with PBS. Nuclei were labeled with 4',6-diamidino-2-phenylindole dihydrochloride (DAPI; TCI Chemicals, Tokyo, Japan). All samples were mounted using VECTASHIELD HardSet Antifade Mounting Medium (H-1400-100, Vector Laboratories, Inc., Newark, CA, USA) and imaged with a confocal microscope (LSM 980, Carl Zeiss, Jena, Germany). Areas positive for cardiac markers were quantified using ImageJ (National Institutes of Health, Bethesda, MD, USA). Sarcomere length was measured using the profile function in ZEN Blue software (version 3.1, Carl Zeiss) on images stained for α-actinin.

2.8 Flow cytometry for apoptosis detection

CiCMs were cultured on TCP, gold nanostructures coated with Matrigel (Mat), or gold nanostructures coated with 200 μg/mL PLL and Matrigel (PMGN). Apoptotic cells were detected using the Alexa FluorTM 488 Annexin V/Dead Cell Apoptosis Kit (V13241, Thermo Fisher Scientific) following the manufacturer's instructions. Briefly, cells were dissociated using trypsin and then allowed to recover for 30 min under standard culture conditions to restore membrane integrity prior to staining. After washing with PBS, cells were stained at room temperature for 15 min with Alexa Fluor 488-conjugated Annexin V and 100 µg/mL propidium iodide (PI). Stained cells were immediately analyzed by flow cytometry using a BD FACSymphonyTM A5 Cell Analyzer (BD Biosciences, Franklin Lakes, NJ, USA). Unstained and single-stained controls were used to set the compensation and gating strategy. Data were processed and analyzed using FlowJo software (FlowJo LLC, Ashland, OR, USA).

2.9 Quantitative real-time polymerase chain reaction

Total RNA was extracted using the TaKaRa MiniBEST Universal RNA Extraction Kit (TaKaRa, Shiga, Japan). Complementary DNA was synthesized from total RNA using a cDNA synthesis kit (TaKaRa). The quantitative real-time polymerase chain reaction (qRT-PCR) was conducted on a QuantStudio3 (Applied Biosystems, Waltham, MA, USA) by combining TaqMan Fast Advanced Master Mix (Applied Biosystems) and TaqMan Gene Expression Assays (Thermo Fisher Scientific). The primers used in this study were as follows: *Cpt1b* (Mm00487191_g1), *Ppara* (Mm00440939_m1), *Tfam* (Mm00447485_m1), *Nfe2 12*

(Mm00477784_m1), Atp2a2 (Mm01201431_m1), Nkx2-5 (Mm01309813 s1), Mef2c (Mm01340842 m1), Mesp1 (Mm00801883_g1), Myh7 (Mm00600555_m1), Cx43 (Mm01179639_s1), Scn5a (Mm01342518_m1), Cacna1c (Mm01188822 m1). The relative gene expression levels were determined using the cycle threshold (Ct) method and normalized against the endogenous reference gene, mouse Gapdh (Mm99999915 g1). In addition, for SYBR Green-based qRT-PCR analysis, reactions were performed on a QuantStudio3 (Applied Biosystems) using PowerUpTM SYBRTM Green Master Mix (Applied Biosystems) and custom oligonucleotide primers (Macrogen, Seoul, Korea). Primer sequences are listed in Table S1. Gene expression was normalized to the reference gene Rplp0. The relative gene expression levels were calculated using the comparative Ct method.

2.10 Evaluation of oxygen consumption rate

The oxygen consumption rate (OCR) of CiCMs was monitored using the XFe96 extracellular flux analyzer (Agilent Technologies, Santa Clara, CA, USA) as an indicator of mitochondrial functionality. On days 8, 12, 15, 19, 22, 26, and 29, CiCMs were seeded at a density of 5×10^4 cells per well in an XFe96 microplate coated with Matrigel. Sensor cartridges were hydrated with XF Calibrant (pH 7.4) for 12 h under non-CO₂, 37 °C conditions 1 day prior to the experiment. After 12 h of seeding, the CiCM medium was aspirated from the wells and the wells were washed twice with XF assay medium. Each well was filled with 180 µL of XF assay medium and incubated at 37 °C in a CO₂-free environment for 30 min. XF assay medium comprised XF DMEM Based Medium (pH 7.4) supplemented with 17.5 mM glucose, 0.5 mM pyruvate, and 2.5 mM glutamine. The assay cartridge, pre-loaded with 2.5 µM oligomycin, 1 µM FCCP, and a combination of 2.5 µM rotenone and 2.5 µM antimycin A, was operated using the Wave 2.6.3 software (Agilent Technologies) following the manufacturer's protocol.

2.11 EC detection for the assessments of mitochondrial functionality in CiCMs

To evaluate mitochondrial functionality, mature CiCMs (days 21–24) were exposed to various mitochondrial inhibitors such as FCCP, oligomycin, rotenone, and antimycin A at concentrations of 0.05 μ M, 0.2 μ M, 2 μ M, 5 μ M, and 10 μ M for 24 h at 37 °C. Following treatment, the CiCMs were rinsed with fresh culture media and incubated for 90 min before DPV detection. Cell viability was then evaluated using the CCK-8 assay according to the manufacturer's protocol.



2.12 Mitochondrial imaging

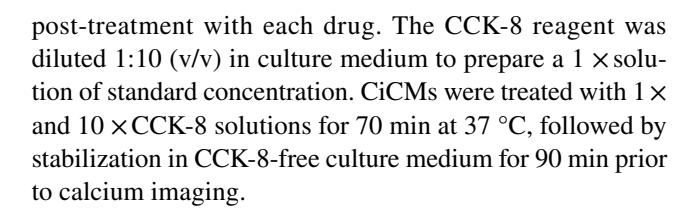
CiCMs plated in confocal dishes (SPL Life Sciences, Gyeonggi-do, Korea) were loaded with 200 nM tetramethylrhodamine, methyl ester (TMRM; #T668, Thermo Fisher Scientific) for 30 min at 37 °C. After thorough washing, they were subsequently incubated with 50 nM TMRM to maintain the equilibrium distribution of the fluorophore, as previously reported [33, 34]. Cells were imaged using a confocal microscope (LSM980, Carl Zeiss) in a live state. CiCMs plated on PMGN were labeled with 500 nM MitoTrackerTM Red CMXRos (#M7512, Thermo Fisher Scientific) for 30 min at 37 °C. The stained cells were washed three times with PBS and fixed with 10% (v/v) formalin solution for 10 min. Cells were then treated with 0.1% (v/v) Triton X-100 for 10 min to achieve permeabilization, blocked with 5% (w/v) BSA for 1 h, labeled with DAPI, washed with PBS, and finally, mounted with VECTASHIELD HardSet Antifade Mounting Medium. Images were acquired using a confocal microscope (LSM980, Carl Zeiss).

2.13 EC detection for functional assessments of CiCMs

To assess the functional changes in CiCMs (day 22–24), the DPV method was employed under identical experimental conditions as those used for living cell detection. Briefly, mature CiCMs were treated with 1, 10, 50, and 100 nM concentrations of ISO and Cch for 10 min. Before EC detection, the culture medium was replaced with fresh medium to prevent potential signal interferences. EC detection was performed at RT. After the DPV detection, cell viability testing was conducted using the CCK-8 kit according to the manufacturer's protocol. Mature CiCMs were incubated with 1× and 10×concentrations of CCK-8 reagent for 70 min at 37 °C, after which the media containing CCK-8 reagent was replaced with fresh medium, and cells were incubated for an additional 90 min before EC detection.

2.14 Calcium imaging

Calcium transient analysis of CiCMs was carried out using 3 μ M Fluo-4 AM (Thermo Fisher Scientific) for 30 min at 37°C. After a single wash with cardiac reprogramming basal medium, serial images of the calcium transients were captured using a confocal microscope (LSM 710, Carl Zeiss). Regions of interest (ROIs) were selected from the acquired images, and changes in fluorescence intensity were plotted using ZEN software (Carl Zeiss). For drug responsiveness testing, CiCMs were exposed to concentrations of 1, 10, 50, and 100 nM of isoproterenol (#420355, Sigma-Aldrich) and carbamoylcholine chloride (#C4382, Sigma-Aldrich). Alterations in calcium transients of CiCMs were monitored



2.15 Contractile function analysis

The contractility of CiCMs was assessed using contraction videos analyzed with the MUSCLEMOTION plugin for ImageJ [35]. Videos were acquired using a CKX53 microscope (Olympus, Tokyo, Japan) and converted into individual TIFF frames using FFmpeg. The extracted frames were imported into MUSCLEMOTION to quantify contraction patterns, including amplitude and frequency. Contraction parameters were calculated as the average of multiple contraction peaks. For electrical stimulation, biphasic pulses (5 V, 1 Hz, and 100 ms) optimized for CiCMs cultured on PMGN were delivered using a WPG100e electrochemical workstation (WonATech, Seoul, Korea).

2.16 Drug cardiotoxicity assessment

On day 21, CiCMs were treated for 24 h with the following compound concentrations: doxorubicin (#15007, Cayman Chemical) at 0.1, 0.5, 1, 5, and 10 µM; remdesivir (#30354, Cayman Chemical) at 1, 3, 6, 9, and 12 µM; rosiglitazone (#71740, Cayman Chemical) at 2, 5, 10, 30, and 50 μM; and liraglutide (#24727, Cayman Chemical) at 0.01, 0.1, 1, 5, and 10 µM, with a subsequent 72-h evaluation of liraglutide. Cells were then washed and incubated with the Cell Counting Kit-8 (CCK-8) reagent. Cell morphology was examined using an optical microscope (Optinity, Korea Lab Technology, South Korea), and cell viability was assessed with the CCK-8 kit and DPV method. The CCK-8 assay was conducted according to the manufacturer's protocol, and absorbance was measured at 450 nm using a microplate reader (Synergy H1 Hybrid Reader, BioTek). Sarcomeric disarray in CiCMs following drug treatment was evaluated using immunofluorescent staining with a mouse anti-αactinin marker.

2.17 Statistical analysis

All quantitative data were expressed as means \pm standard deviations (SD). The "n" values shown in figure legends represent biological replicates. Statistical differences between groups were determined using a two-tailed unpaired t-test, one-way or two-way ANOVA followed by Tukey's post hoc test, using Prism 8 software (GraphPad, La Jolla, CA, USA). Differences were deemed statistically significant when the p-value was less than 0.05. All quantitative EC results are



presented as mean \pm SD from three replicates. Significant differences are denoted as *(p<0.05) or **(p<0.01) using the unpaired Student's t-test. Multiple comparisons were performed using one-way ANOVA coupled with Tukey's post hoc test.

3 Results and discussion

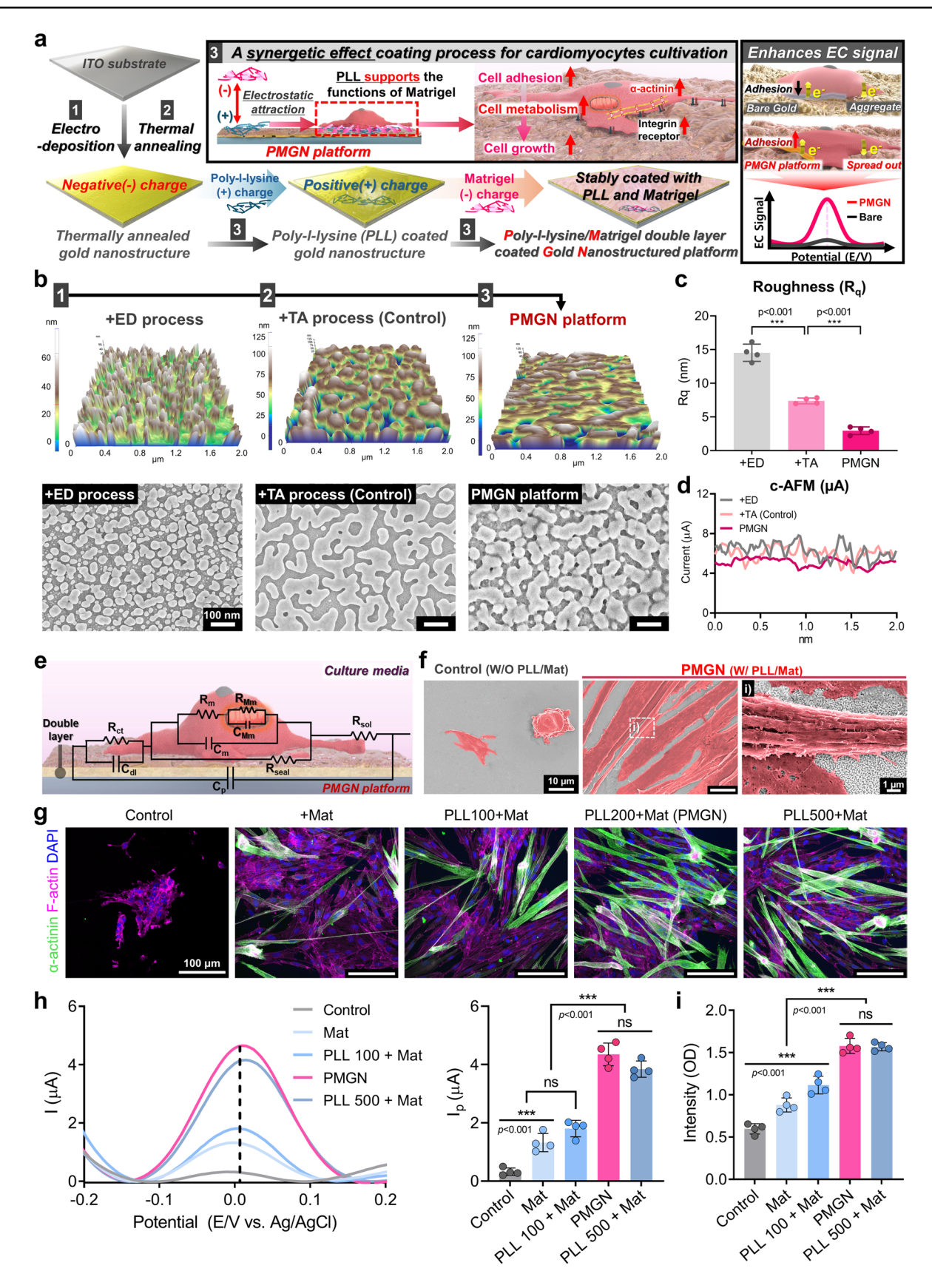
3.1 Development of a PMGN composites for enhanced cell adhesion and EC detection of CiCM metabolic activity

To monitor the dynamics of cellular metabolism in CiCMs using EC detection, we developed an electrochemically deposited gold nanostructure composites coated with PLL and Mat for CiCMs. During the development of the PMGN composites, the highly conductive ITO substrate undergoes three processing steps: (i) electrodeposition (ED), (ii) thermal annealing (TA), and (iii) PLL/Mat coating. These steps improve the culture conditions of CiCMs by enhancing their adhesion to the PMGN composites (Fig. 2a). To compensate for the low electrocatalytic properties of ITO, a gold film in nanostructured form, offering an increased active surface area, was fabricated to enable EC detection of dynamic intracellular redox reactions in CiCMs. ED times for a gold mixture solution on the ITO substrate were optimized, and the resulting morphology and surface characteristics were analyzed using field-emission scanning electron microscopy (FE-SEM) and atomic force microscopy (AFM). Consequently, a deposition time of 180 s was established as the optimal condition, forming gold nanoparticles with a high active surface area and the smallest size variations for EC detection compared to 60 s, 120 s, and 360 s groups (Figs. 2b and S1a). Despite the benefits of generating gold nanostructures via the ED process, a significant challenge remains the weak adhesion of the gold film to the ITO-coated substrate, which is essential for long-term monitoring of CiCM conversion and maturation. To address this issue, the TA process was applied and optimized, which involves restructuring the atoms within a single nanoparticle without direct contact; Ostwald ripening [36] causes two nanoparticles to merge upon contact to form a single, larger nanoparticle, and coalescence in metal nanostructures under optimal conditions $(T=100 \, ^{\circ}\text{C} \text{ and } t=10 \, \text{min}) \, [37]$, while varying the time and temperature conditions, to address this instability (Figs. 2b and S1b). Next, to promote CiCM adhesion on our platform, we employed PLL, a strongly positively charged polymer, and Mat, an ECM-based hydrogel (Fig. S2a). Optimization of PLL concentration and Mat coating conditions involved coating the TA-processed platform with varying PLL concentrations (0, 100, 200, and 500 µg/mL) followed by Mat application. The combination of 200 µg/mL PLL and Mat provided optimal conditions, significantly improving cell adhesion on the PMGN composites (Fig. 2b). AFM revealed a 59.96% reduction in surface roughness, a measure of structural height variations, compared to the uncoated control (Fig. 2c). Conductivity analysis using c-AFM demonstrated minimal signal variation (1.59 µA), confirming that PLL and Mat coatings did not impair platform conductivity (Figs. 2d and S2b). For the circuit design on the PMGN composites for CiCM detection, it was previously established that active cellular redox reactions, especially those involving mitochondria [23], are crucial for generating electrical signals at a specific potential $(E_p = 0 \text{ V})$, which subsequently influences contact resistance (R_{seal}) and mitochondrial membrane resistance $(R_{\rm Mm})$. Consequently, the $R_{\rm seal}$ value, indicative of the cell-electrode interface, becomes negligible (Fig. 2e) [38].

When cultured on the PMGN platform for 4 days following 19 days of reprogramming, CiCMs with PLL200 + Mat coating demonstrated enhanced adhesion and spreading, while control cells formed compact clusters with limited spreading (Fig. 2f). Further assessment revealed that only PLL200 + Mat and PLL500 + Mat coatings supported an increased number of α -actinin-positive cardiomyocyte-like cells, whereas other groups (Control, + Mat, and PLL100 + Mat) exhibited poor adhesion and resultant aggregation with low α -actinin expression (Figs. 2g and S2c–f). These findings underscore the importance of combining PLL and Mat for stable adhesion and spreading of reprogrammed cardiomyocyte-like cells.

Following the confirmation of stable CiCMs cultivation on the PMGN composites, differential pulse voltammetry (DPV) analysis was conducted (Figs. 2h and S2g). The PLL 200 + Mat group exhibited a 13.54-fold increase in DPV signal intensity and a 2.64-fold increase in cell numbers, as determined by CCK-8 assay results, compared to the uncoated control (Fig. 2h, i). The correlation between electrical signals and cell viability demonstrates the sensitivity of the EC method, as the DPV signal for the PMGN group was 5.13 times higher than that of the control group, outperforming the conventional CCK-8 assay. This heightened sensitivity differentiated between the PLL200 + Mat and PLL500 + Mat groups, confirmed by immunostaining, which the CCK-8 assay could not detect. To further validate the biosafety of the PMGN platform (PLL200 + Mat), considering the potential cytotoxicity of PLL at high concentrations, we conducted an additional analysis using Annexin V/PI staining. Flow cytometry revealed that CiCMs cultured on PMGN exhibited a higher proportion of viable cells (87.73%) and lower apoptotic cell levels (9.15%) compared to the TCP and Mat groups, while necrotic cell proportions remained low and comparable across all conditions (Fig. S3). These results confirm that the 200 µg/mL PLL used in the PMGN platform does not disrupt membrane







∢Fig. 2 Development and characterization of the PMGN platform. **a** Schematic of the PMGN platform development and its adhesive capabilities. b AFM images of the fabrication processes for the PMGN platform alongside FE-SEM images of electrodeposited (ED) gold nanostructure (180 s), thermally annealed (TA) gold nanostructure at 100 °C for 10 min, and the PMGN platform (scale bars = 100 nm). \mathbf{c} Root mean square roughness (R_a) analysis for EC process, TA process (control), and the PMGN platform groups (n = 4). d Results from c-AFM image analysis (Fig. S2b). e Schematic illustration of the circuit flow in the EC detection components of our system. C_{dl} : capacitance of the electrical double layer; C_{m} : capacitance of the cell membrane; R_{sol} : resistance of culture media; R_{ct} : charge transfer resistance; $R_{\rm seal}$: resistance of CiCM-PMGN distance; $R_{\rm m}$: resistance of the cell membrane; $R_{\rm Mm}$: resistance of the mitochondrial membrane in CiCM; $C_{\rm Mm}$: capacitance of the mitochondrial membrane in CiCM; $C_{\rm p}$: parasitic capacitance. **f** FE-SEM images of CiCMs (day 23) for each group at control and on the PMGN platform (scale bars = 10 μm). Enlarged FE-SEM image in the PMGN platform (i) (scale bars = 1 µm). g Immunofluorescence images of CiCMs, cultured on the PMGN platform with different concentrations of PLL and Matrigel coatings, showing α -actinin and F-actin expression (scale bars = 100 μm). h DPV measurements of CiCMs (day 23) under various coating conditions (left panel) and the quantification of the DPV results presented as a bar graph (right panel) (n = 4). i Cell viability tests for CiCMs cultured under various coating conditions (n = 4). Statistical significance between groups was determined using a one-way ANOVA followed by Tukey's multiple comparisons test (*p < 0.05, **p < 0.01, and ***p < 0.001). Data are presented as mean \pm S.D

integrity or induce cytotoxicity, supporting its suitability for sensitive electrochemical measurements.

Furthermore, the long-term stability of the PMGN platform was systematically evaluated. The results demonstrate that although limited surface erosion of the PLL/Mat layer occurs over a 30-day period, the PMGN platform retains structural integrity, electrical conductivity, electrocatalytic activity, and the ability to detect cell-specific EC signals. These findings validate the reliability and functional robustness of PMGN platform for long-term monitoring applications (Fig. S4).

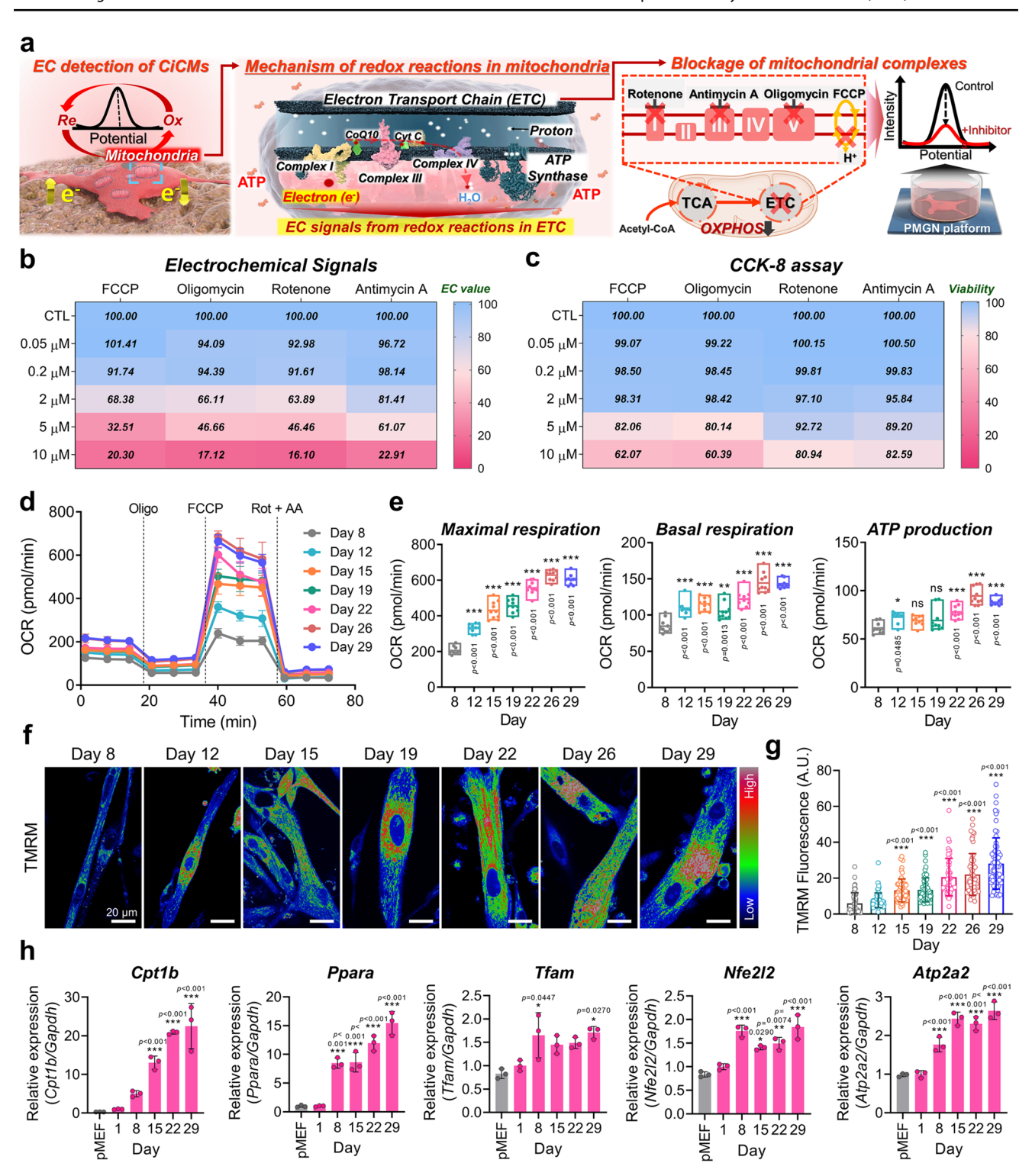
3.2 Redox reactions from mitochondrial metabolism generate the electrical signals in CiCMs

Having demonstrated that the PMGN platform can reliably monitor cellular processes in CiCMs, we further investigated the mechanism for EC detection of mitochondrial metabolism, particularly OXPHOS, by examining intracellular redox reactions and assessing how mitochondrial inhibitors modulate these reactions and alter resultant electrical signals (Fig. 3a). To evaluate the impact of mitochondrial inhibitors on cellular redox activity, CiCMs were treated with compounds targeting various mitochondrial complexes, such as rotenone (complex I), antimycin A (complex III), oligomycin (complex V), and carbonyl cyanide-*p*-trifluoromethoxyphenylhydrazone (FCCP; disrupts the proton gradient and decouples electron transport from ATP synthesis). These

effects were analyzed at different concentrations using the EC detection and the CCK-8 assay (Figs. 3b, c and S5). The PMGN composites demonstrated a highly sensitive response to the mitochondrial inhibitors, starting at concentrations as low as 2 μ M, with changes in EC signals ranging from 18.59 to 36.11%. Conversely, the CCK-8 assay, which indirectly measures cell viability through mitochondrial dehydrogenase activity, exhibited only minor fluctuations in the range of 1.58 to 4.16% at these concentrations (Fig. 3b, c). These results demonstrate that the PMGN composites offer superior sensitivity in detecting mitochondrial dysfunction as they directly capture variations in electron transfer linked to mitochondrial redox reactions. This enhanced detection capability enables more precise and sensitive measurements of mitochondrial activity compared to traditional methods.

To further verify the EC method for monitoring mitochondrial activities in CiCMs, changes in the OCR were monitored over 29 days during direct cardiac reprogramming (Fig. 3d). As mitochondrial metabolism intensified, OCR values for maximal respiration, basal respiration, and ATP production rose by 2.92-fold, 1.69-fold, and 1.43-fold, respectively, by day 29 compared to day 8, indicating significant metabolic maturation in CiCMs (Fig. 3e). To further explore the relationship between mitochondrial activity (i.e., OXPHOS) and CiCM maturation, mitochondrial membrane potential ($\Delta \Psi_{\rm M}$) was measured over 1 month using tetramethylrhodamine methyl ester (TMRM) staining (Figs. 3f, g and S6). $\Delta \Psi_{\rm M}$, generated by proton pumps in complexes I, III, and IV, is critical for energy storage during OXPHOS and plays a vital role in CiCM maturation [39, 40]. Consistent with the OCR results depicted in Fig. 3e, $\Delta\Psi_{M}$ increased 4.71-fold by day 29 compared to day 8 (Fig. 3g). Furthermore, an analysis of mitochondrial mass in CiCMs on PMGN using Mito-Tracker red staining showed a 13.31-fold increase by day 29 relative to day 8 (Fig. S7). Subsequently, to monitor the maturation of CiCMs, the expression of genes associated with metabolism (Cpt1b, Ppara, Tfam, Nfe2 l2, Atp2a2) was examined over a 29-day period (Fig. 3h). Cpt1b is instrumental in regulating the β-oxidation pathway by facilitating the transport of longchain fatty acids into mitochondria [41–43], while *Ppara* serves as a crucial regulator of mitochondrial fatty acid oxidation and metabolic homeostasis [44–46]. *Tfam* supports mitochondrial DNA replication and transcription [47, 48], while Nfe2 12 preserves cellular redox homeostasis, impacting mitochondrial membrane potential and ATP synthesis [49, 50]. Atp2a2 regulates the movement of calcium ions critical for muscle contraction and energy metabolism [51]. Over time, the expression levels of these genes increased, peaking on day 29. Particularly, Cpt1b and Ppara, crucial β-oxidation genes, exhibited significant upregulation, with increases of 22.49-fold and 15.45-fold by day 29 compared to day 1. This upregulation signifies that CiCMs become metabolically more mature over time, increasingly depending





on β-oxidation and OXPHOS for energy. To ensure that the observed upregulation patterns were not affected by potential metabolic responsiveness of the reference gene *Gapdh*, we additionally performed qRT-PCR using *Rplp0*, a commonly used housekeeping gene with stable expression across metabolic states [52–54]. This analysis confirmed consistent upregulation trends for key metabolic markers (*Cpt1b*,

Ppara) (Fig. S8). Traditional methods, as demonstrated in Fig. 3d–h, effectively analyzed these metabolic shifts and monitored CiCM maturation throughout the 29-day period. Although these methods are powerful analytical tools, they are inherently invasive and destructive, which precludes the reuse of CiCMs.



∢Fig. 3 Electrical signals rely on the redox reactions of mitochondrial metabolism. a A schematic representation of EC detection in CiCMs and the control of electrical signals through mitochondrial inhibitors. **b** Heatmap depicting electrical signals in CiCMs (n = 3) following the administration of mitochondrial inhibitors, derived from Fig. S5a (DPV graph). c Heatmap showing CCK-8 results (n = 3) post mitochondrial inhibitor treatment. d Measurement of OCR in CiCMs on each respective day using an XFe96 extracellular flux analyzer (n = 10). OCR readings were taken over 72 min. At 16 min, 2.5 µM Oligomycin (Oligo) was administered, followed by 1 µM FCCP at 35 min, and finally a mixture of 2.5 µM rotenone and 2.5 µM antimycin A (Rot + AA) at 55 min. e Quantitative analysis of maximal respiration (n = 10), basal respiration (n = 10), and ATP production (n = 10)10) derived from OCR findings. f Pseudo-colored images of TMRM staining employed to analyze the increase in mitochondrial membrane potential $(\Delta \Psi_M)$ in CiCMs over time, with the reference bar indicating red for high $\Delta \Psi_M$ and blue for low $\Delta \Psi_M$ cells (scale bars = 20 μm). g Quantification of relative TMRM fluorescence intensity in CiCMs using TMRM confocal images ($n = 54 \sim 76$). Statistical significance between groups was determined using one-way ANOVA followed by Tukey's multiple comparisons test (*p< 0.05, **p< 0.01, and ***p < 0.001 versus Day 8 group). **h** qRT-PCR analysis of cardiac-related mRNA expressions in CiCMs cultured on a PMGN platform (n = 3, one-way ANOVA followed by Tukey, *p < 0.05, **p < 0.050.01, and ***p< 0.001 versus day 1 group). Data are presented as means \pm S.D

3.3 Non-destructive in situ EC monitoring and assessment of CiCM reprogramming using the PMGN platform

The PMGN composites were employed to monitor mitochondrial redox dynamics throughout the entire direct reprogramming process into CiCMs, capturing critical transitions from a fibroblast-like state to cardiomyocyte-like cells (Fig. 4(a)). Initial validation involved comparing the expression of key cardiac markers in CiCMs cultured on TCP through immunostaining with the metabolic and electrical signals detected by the PMGN composites (Figs. S9 and S10). During the initial 6 days of reprogramming, CiCMs exhibited significant changes in key cardiac proteins, including α-actinin, cardiac troponin-T (cTnT), and Gata4. A notable observation was the 51.24% increase in the early cardiac marker Gata4 [55-57] from day 1 to day 3, followed by a decline starting on day 3 (Figs. S9a, b), while α-actinin and cTnT levels increased (Fig. S9c). These transitions indicate rapid transdifferentiation toward a cardiomyocyte-like phenotype. The electrical signals recorded by the PMGN platform mirrored these early-stage changes, showing a 312.32% increase from day 1 to day 3, followed by a 23.38% decrease on day 4, before rising again on day 5 (Fig. S10). These results demonstrate that the PMGN platform effectively captures early-stage transdifferentiation dynamics, potentially unveiling metabolic shifts more dramatically than structural protein expression, such as α-actinin and cTnT.

Building on these early-stage findings, the PMGN platform was further employed to monitor the maturation process over a 29-day period (Fig. S11). As illustrated in Fig. 4(b), pMEFs consistently exhibited low CV signals, likely due to their minimal reliance on OXPHOS. During the direct cardiac reprogramming process, fibroblasts primarily utilize glycolysis for energy production [27]. As these cells transition into cardiomyocyte-like cells, they undergo a metabolic shift, favoring OXPHOS in the mitochondria to accommodate the increased energy demands essential for cardiomyocyte functions, particularly contraction [28]. This transition from glycolysis to OXPHOS is crucial for reprogramming efficiency and the functional maturation of CiCMs. Unlike pMEFs, CiCMs showed a clear maturationdependent increase in EC signals, distinctively separating the early reprogramming state on day 2 from the more mature state observed by day 22. From day 5 to day 12, EC signals remained relatively stable, indicating an initial stabilization phase of reprogramming (Fig. 4(c, d)). However, between days 12 and 22, EC signals significantly increased. By day 15, the signals had increased by 50.99% compared to day 12, and by day 22, the increase had reached 146.55%, possibly indicating a critical transition in the maturation process. The pMEF signals remained consistently low and did not interfere with the EC signals observed in CiCMs throughout the 29-day period (Fig. 4(c)). Immunostaining of CiCMs cultured on the PMGN platform revealed that α-actinin-positive cells exhibiting cross-striated patterns began to appear as early as day 5 of cardiac reprogramming, with more pronounced sarcomere structures observed by day 19 (Fig. 4(e, f)). Over the 29-day period, α-actinin-positive CiCMs also demonstrated clearer and more frequent development of transverse tubules (t-tubules), confirmed by wheat germ agglutinin (WGA) labeling (Fig. 4(e, g)). The findings indicate a strong correlation between increased mitochondrial activity, as detected through EC signals, and the maturation of cardiomyocytes. By monitoring mitochondrial redox reactions, the PMGN platform correlates these metabolic shifts with structural developments, such as sarcomere formation and t-tubule organization, enabling earlier and more precise evaluation of cardiomyocyte maturation compared to conventional methods. Unlike conventional methods that provide static snapshots, the PMGN platform facilitates continuous, in situ monitoring, offering a more accurate and dynamic assessment of cellular transitions over both shortand long-term periods in a non-destructive manner.

To further investigate the influence of PMGN surface properties on cardiomyocyte development (i.e., physical cues), the maturation of CiCMs was assessed through immunostaining and PCR (Fig. 4(f–h)). In the TCP group, CiCMs successfully exhibited distinct striated patterns characteristic of mature cardiomyocytes for 29 days (Figs. S12, S13). By day 19, the sarcomere length in CiCMs on TCP reached approximately 2.2 μm , akin to that in adult cardiomyocytes, indicating that structural



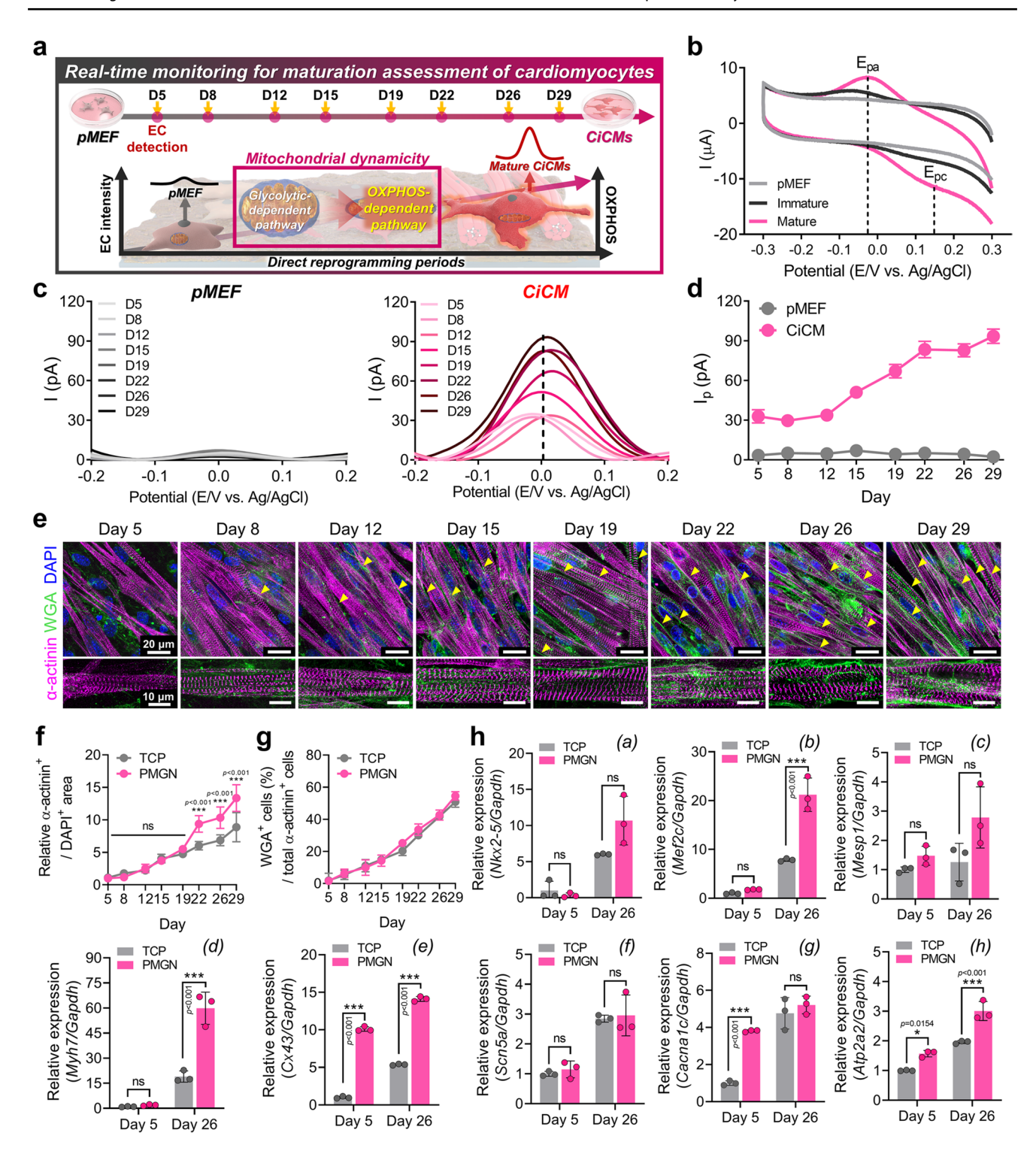


Fig. 4 Maturation assessments for CiCMs using electrochemical detection of intracellular dynamics. (a) Schematic of real-time monitoring for direct cardiac reprogramming and mitochondrial dynamics. (b) CV graph comparing immature CiCMs (day 2) with mature CiCMs (day 18) on the PMGN platform. (c) DPV signals from pMEF (left-panel) and CiCMs (right-panel) cultured for 29 days on the PMGN platform. (d) Line graph representing the electrical signals calculated from c (n= 3). (e) Immunofluorescent staining for α-actinin and t-tubules (detected by WGA) in CiCMs on the PMGN platform, for each respective day (upper image scale bars = 20 μm, lower image

scale bars = 10 μ m). Yellow arrows highlight distinct t-tubules. (f) Quantification of α -actinin⁺ area $(n=7\sim9)$, (g) cells exhibiting t-tubule structures (n=6) as indicated by α -actinin and WGA staining. (h) qRT-PCR analysis of cardiac-specific genes in CiCMs cultured on TCP and PMGN at days 5 and 26 (n=3). Data are presented as means \pm S.D. Statistical significance between groups was determined using two-way ANOVA followed by Tukey's multiple comparisons test (*p<0.05, **p<0.01, and ***p<0.001 versus TCP group)



maturation had occurred (Fig. S12) [58]. These structural changes in CiCM development and maturation were similar to those seen in CiCMs on the PMGN platform. Additionally, the incidence of CiCMs displaying pronounced t-tubules was nearly identical in both the TCP and PMGN groups (Fig. 4(g)). Cardiac-specific gene expression in the TCP and PMGN groups was further examined by qPCR on days 5 and 26 (Fig. 4(h)). Early cardiac transcription factors involved in cardiomyocyte lineage specification and initial development, such as Nkx2-5, Mef2c, and Mesp1, exhibited similar expression levels in both groups on days 5 and 26, except for *Mef2c*, which showed elevated expression in the PMGN group on day 26 (Fig. 4(h(a-c))). Unexpectedly, markers of cardiomyocyte maturation, including Myh7 (sarcomere formation) and Cx43 (gap junctions), demonstrated significantly higher expression levels on day 26 in the PMGN group compared to the TCP group (Fig. 4(h(d, e))). Conversely, Scn5a (sodium channels) and Cacna1c (calcium channels) showed similar expression levels between the two groups (Fig. 4(h(f, g))). Notably, ATP2a2, crucial for calcium handling in mature cardiomyocytes, was more highly expressed in CiCMs on the PMGN platform by day 26 (Fig. 4(h(h))). These unexpected findings suggest that the PMGN platform not only supports cardiomyocyte differentiation but also enhances advanced maturation, particularly in terms of calcium regulation and structural organization, surpassing the outcomes observed in the TCP group.

To evaluate whether CiCMs cultured on the PMGN platform exhibit functional cardiomyocyte-like properties, we analyzed their spontaneous contractile activity and responsiveness to electrical pacing (Fig. S14). Time-lapse imaging of intracellular Ca²⁺ influx using Fluo-4 AM demonstrated consistent calcium transients and rhythmic beating activity in CiCMs on both TCP and PMGN, indicating stable spontaneous contractile function (Fig. S14a). Subsequent MUSCLEMOTION analysis confirmed no significant differences in beats per minute (BPM), peak-to-peak time, and contraction amplitude between CiCMs on TCP and PMGN, suggesting that both substrates support comparable spontaneous contractility (Fig. S14b, c). Importantly, CiCMs on PMGN responded reliably to 1-Hz electrical pacing, exhibiting synchronized contractions with a BPM of 60.15 ± 0.52 and a peak-to-peak interval of 1.00 ± 0.04 s (Fig. S14 d, e, and Supplementary Movie 1). These findings provide functional evidence that CiCMs on the PMGN platform not only undergo metabolic and structural maturation but also acquire electrophysiological responsiveness, thereby underscoring the utility of PMGN as a functional assessment platform for reprogrammed cardiomyocyte-like cells.

3.4 Electrophysiological function analysis of CiCMs via EC methods

While the PMGN platform has demonstrated potential for long-term cultivation and maturation assessment of CiCMs, a precise functional assessment of mature CiCMs, especially their electrophysiological properties, remains to be elucidated. To investigate this, we explored whether the PMGN platform could detect drug responses by assessing the effects of β-adrenergic and muscarinic stimulation on CiCMs through EC detection and compared these results with those from calcium transient measurements. ISO and Cch alter intracellular calcium levels in cardiomyocytes, directly linked to mitochondrial activity and OXPHOS. ISO activates β -adrenergic receptors (β -AR), which stimulate adenylate cyclase to catalyze the conversion of intracellular ATP to cyclic AMP (cAMP) [59, 60]. This process activates protein kinase A (PKA), which then phosphorylates L-type calcium channels (LTCC) in the sarcoplasmic reticulum (SR), elevating intracellular calcium levels [61, 62]. The increase in calcium enhances mitochondrial OXPHOS, boosting ATP production, which supports contractility and raises the CiCM beating rate [63]. Conversely, Cch interacts with muscarinic acetylcholine receptors (mAchR), reducing cAMP levels and PKA activity, which decreases calcium influx [64]. Consequently, this reduction in calcium influx decreases mitochondrial OXPHOS and ATP production, lowering the beating rate (Fig. 5a).

As hypothesized, applying ISO and Cch to CiCMs cultured on the PMGN platform for 10 days induced remarkable dynamic changes in OXPHOS activities, resulting in measurable alterations in electrical signals (Fig. 5b, c). These dynamics were compared with the results from the CCK-8 assay and calcium transient to assess cell viability and functions, such as beats per minute (BPM) (Fig. 5d-f). The electrical signals and cell viability were quantified at various concentrations of ISO and Cch treatments. It was found that the PMGN platform elicited precise functional assessments from 50 nM of both drugs (ISO and Cch) without damage to cell viability. Interestingly, despite no changes in cell viability, we observed significant fluctuations in electrical signals in mature CiCMs treated with ISO (22.07% increase) and Cch (20.92% decrease) at a concentration of 100 nM (Fig. 5c, d). Similarly, we investigated the responsiveness of CiCMs (days 22-24) treated with ISO and Cch, which influenced cardiomyocyte beating rates (Fig. 5e, f). Notably, the frequency of Ca^{2+} transients (104.9% $\pm 21.9\%$ at 10 nM and $146.5\% \pm 16.9\%$ at 100 nM) increased, with a more pronounced BPM increase observed at higher ISO concentrations. In contrast, opposite trends in the frequency of Ca²⁺ transients (73.9% \pm 13.3% at 10 nM and 50.8% \pm 10% at 100 nM) were observed with higher Cch concentrations. These results indicate that the PMGN platform can accurately and



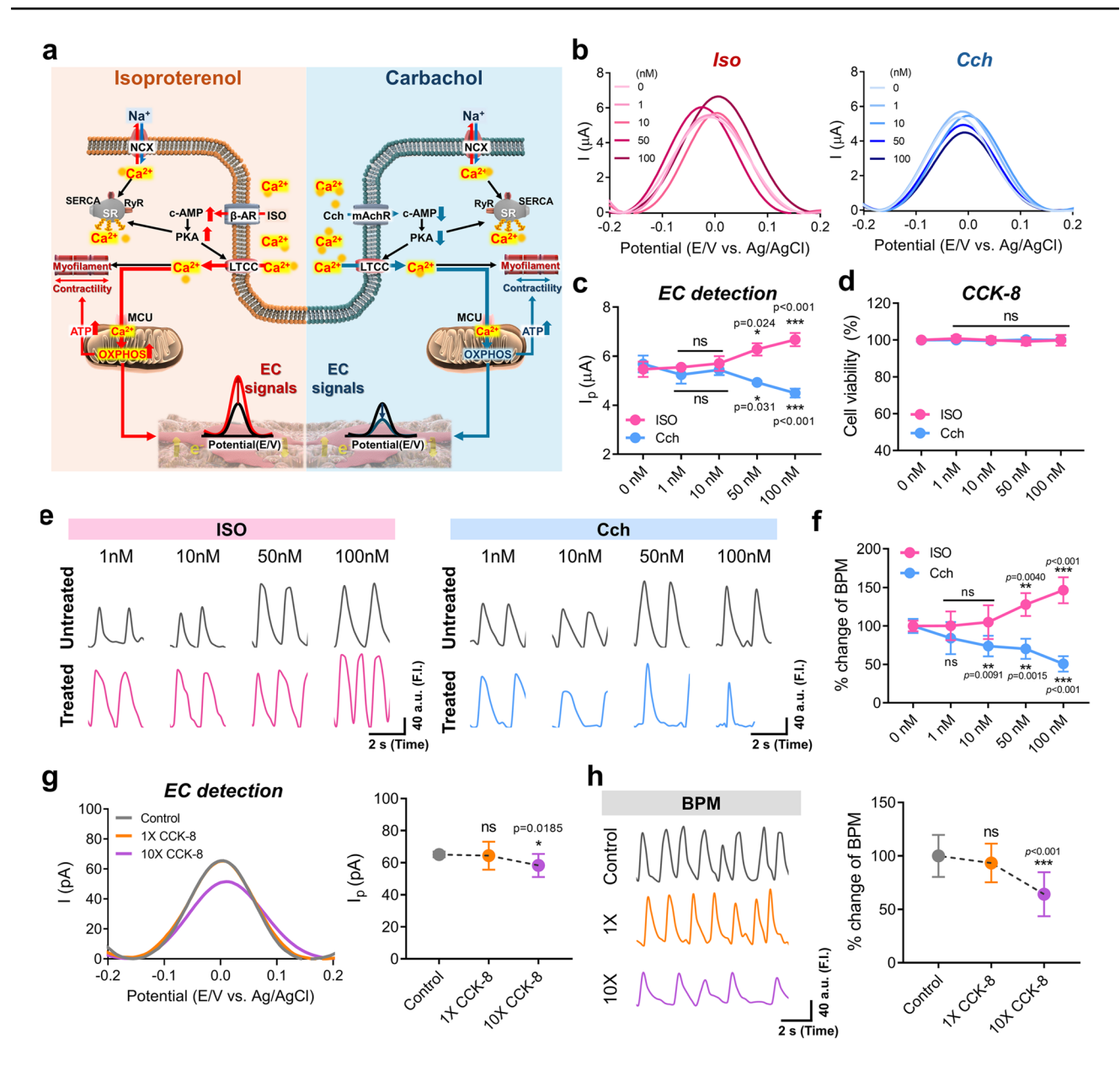


Fig. 5 The PMGN platform evaluates the electrophysiological functions in CiCMs. **a** Schematic illustrating the actions of isoproterenol (ISO, left) and carbachol (Cch, right) in CiCMs. **b** DPV graphs from CiCMs exposed to ISO (left panel) and Cch (right panel) for 10 min at concentrations ranging from 1 to 100 nM. **c** Quantified electrical signals from DPV results in iCMs exposed to both ISO and Cch (n = 3). **d** CCK-8 assay results of CiCMs treated with ISO and Cch after EC detection (n = 3). Statistical significance across groups was determined using one-way ANOVA followed by Tukey's multiple comparisons test (*p < 0.05, **p < 0.01, and ***p < 0.001). Data are expressed as means \pm S.D. **e** Representative patterns of Ca²⁺ fluorescence alterations as a function of ISO and Cch concentrations. **f**

Changes in BPM of CiCMs exposed to various doses of ISO and Cch, normalized against the untreated control (n=10, two-way ANOVA followed by Tukey, **p < 0.01 and ***p < 0.001 versus 0 nM control group within each drug). **g** DPV graph of CiCMs treated with 1× and 10 × CCK-8 reagents for 70 min. And the quantified results of electrical signals from the left panel (n=3). **h** Representative patterns of Ca²⁺ fluorescence variations as a function of 1× and 10 × CCK-8 reagents. And BPM of CiCMs treated with 1× and 10 × CCK-8 reagents, normalized against the untreated control (n=25, two-tailed t-test, ***p < 0.001 versus control group). Data are presented as means \pm S.D

sensitively detect functional changes in mature CiCMs associated with OXPHOS-mediated processes, such as responses to β -adrenergic and muscarinic signaling, providing an alternative to calcium imaging. Consequently, the results of EC

detection and Ca²⁺ transient measurements displayed a similar trend (Fig. 5c, f).

Next, we examined the effects of CCK-8 reagent on CiCMs over 24 h at $1 \times$ and $10 \times$ concentrations by tracking



changes in electrical signals and calcium transients (Fig. 5g, h). No significant changes in electrical signals or BPM were observed at 1 × CCK-8 concentration. However, at a 10 x concentration, there was a decrease in BPM and electrical signals, suggesting that the reagent, commonly used for colorimetric detection of cell viability, may induce cardiac toxicity at high concentrations. In contrast, the proposed EC detection using the PMGN platform eliminates the need for external reagents, thereby avoiding the potential risk of toxicity associated with reagents in colorimetric assays. These results collectively indicate that the PMGN platform can effectively monitor cardiomyocyte maturation and functional changes driven by mitochondrial metabolism in response to β-adrenergic and muscarinic stimulation. By detecting dynamic shifts in mitochondrial activity following drug exposure, the platform can sensitively capture electrophysiological changes without compromising the underlying cellular state.

3.5 Cardiotoxicity assessment using EC methods

Given its proven ability to assess CiCM maturation and function, the PMGN platform was further adapted for high-throughput drug screening to evaluate cardiotoxicity. We hypothesized that, owing to its high sensitivity, the PMGN platform combined with the EC method would facilitate early detection of drug-induced cardiotoxic effects. Four drugs were selected for evaluation: (i) the anti-cancer agent doxorubicin [65–67]; (ii) the COVID-19 therapeutic remdesivir [68, 69]; (iii) the diabetes drug rosiglitazone [70, 71]; and (iv) the type 2 diabetes and chronic obesity therapeutic liraglutide (Fig. 6a) [72, 73].

The DPV signals sourced from CiCMs indicated that doxorubicin, remdesivir, and rosiglitazone cause cardiotoxic effects, whereas liraglutide did not show a significant decrease in signal intensity, suggesting an absence of cardiotoxicity (Fig. 6b). These observations were consistent across various concentrations (0–10 μM) under both 24-h and 72-h treatment conditions. These findings were substantiated by cell viability assessments and sarcomere structure analysis. Specifically, doxorubicin caused a 5.47% decrease in electrical signal at a low concentration of 0.1 µM, a change not detectable using the CCK-8 assay (Fig. 6c, d). Cellular damage was apparent at concentrations of 1 µM, as shown by immunostaining and CCK-8 assay, which highlighted sarcomeric disarray with unclear α -actinin striated patterns and a reduction in cell viability (Fig. 6d, e). At this concentration, electrical signals decreased by a significant 30.12%, indicating exceptional sensitivity in detecting changes in cardiac cell viability and function (Fig. 6c). Remdesivir exhibited cardiotoxicity at concentrations above 3 µM as assessed by both the PMGN platform and conventional assays (Fig. 6c, e). At 6 μM, EC signals decreased by 50.55% along with a 26.11% reduction in cell viability and sarcomere disruption. Rosiglitazone displayed cardiotoxic effects more rapidly, evidenced by a 23.46% decrease in EC signal at 2 µM (Fig. 6c), while the CCK-8 assay indicated only a 7.32% reduction in cell viability (Fig. 6d). In contrast, the liraglutide group exhibited no significant changes in either EC signals or conventional assays (Figs. 6c-e and S15). These results illustrate that the EC method offers superior sensitivity in detecting early-stage cardiotoxic effects compared to conventional assays. Significant changes in electrical signals were noted at lower drug concentrations, whereas traditional methods necessitated higher concentrations and more extensive cellular damage. With its rapid, reagent-free assessments (less than 30 s), the PMGN platform provides a high-throughput and effective solution for cardiotoxicity screening in preclinical drug evaluations.

4 Conclusions

The PMGN composite platform was developed to monitor real-time mitochondrial dynamics during direct cardiac reprogramming via EC methods. This label-free, non-destructive approach allows for precise assessments of cell maturity, functionality, and cardiotoxicity in CiCMs. By tracking cellular energy metabolism, intrinsically linked to cardiac maturation and functional competency, the platform facilitates a more accurate and efficient evaluation of metabolic shifts throughout the maturation process, all without necessitating cell destruction.

EC analysis used in this study identifies redox reactions during mitochondrial metabolism, proving highly effective for evaluating the metabolic dynamics of CiCMs. Mature CiCMs at day 22 demonstrated a 153.55% increase in electrical signals compared to their immature counterparts at day 5, showing the platform's high sensitivity for detecting metabolic shifts during reprogramming and maturation. Furthermore, the platform was highly effective in assessing functional changes induced by β-adrenergic and muscarinic stimulation. Treatment with ISO and Cch at 100 nM resulted in significant changes in electrical signals—an increase of 22.07% with ISO and a decrease of 20.92% with Cch—illustrating the platform's capability to monitor mitochondrial activity shifts, even without detectable changes in cell viability. This sensitivity indicates that the PMGN composite platform could accurately evaluate cardiomyocyte functionality and drug responsiveness. The ability of the platform to detect drug-induced cardiotoxicity early, as demonstrated by the detection of toxic effects from doxorubicin and remdesivir, further underscores its utility.

In clinical translation, guidelines for cell therapy development emphasize the need for comprehensive functional and safety assessments of therapeutic cells [74, 75]. While



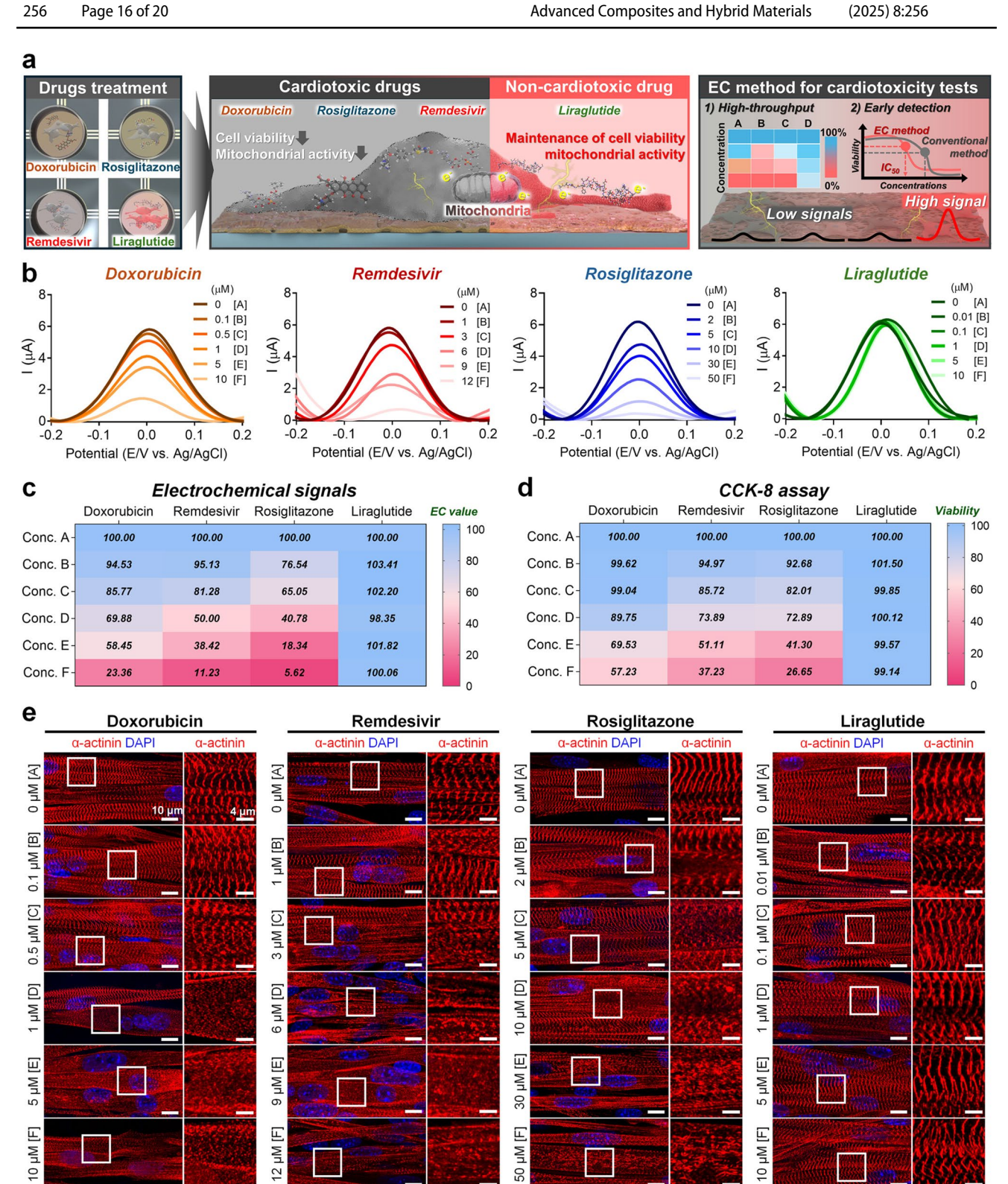


Fig. 6 Application for cardiotoxicity assessment using the PMGN platform. a Scheme of cardiotoxicity testing using the EC method. b DPV graphs of CiCMs exposed to doxorubicin, remdesivir, rosiglitazone, and liraglutide at various concentrations for 24 h. c Heatmap of electrical signals obtained from b (n=3). d Heatmap of CCK-8

results on CiCMs exposed to doxorubicin, remdesivir, rosiglitazone, and liraglutide at various concentrations for 24 h (n = 3). e Immunofluorescence image of α -actinin in CiCM groups exposed to multiple doses of doxorubicin, remdesivir, rosiglitazone, and liraglutide for 24 h (scale bars = $10 \mu m$ and $4 \mu m$ for magnified images)



traditional assays like viability tests, molecular profiling, and immunohistochemistry staining are essential, they are often destructive and time-consuming, making them poorly suited for real-time monitoring and efficient feedback during cell preparation. The PMGN composite platform provides a complementary solution by enabling real-time, non-invasive tracking of functional and metabolic changes, thereby ensuring effective quality control during cell preparation. This system has the potential to streamline the monitoring process and ensure that the utilized cardiomyocytes are functionally mature. By detecting subtle shifts in mitochondrial metabolism, the PMGN composite platform offers immediate feedback, enabling rapid adjustments. This approach can significantly enhance clinical workflows by ensuring regulatory compliance, reducing the time to therapy for patients, and improving quality control during cardiotoxicity testing.

Overall, the PMGN composite platform provides a robust, real-time alternative to traditional methods for evaluating cardiomyocyte maturation, functionality, and drug response, thereby enhancing the preparation and quality control of stem cell-based therapies. In addition, the PMGN platform can be readily expanded to multi-well formats, enabling high-throughput screening and standardized evaluation of stem cell-derived cardiomyocytes under clinical conditions. This expandability supports large-scale and reproducible metabolic assessments, highlighting its potential utility in clinical translation (Fig. S16), particularly for the validation and safety monitoring of cardiomyocyte products in regenerative medicine [76, 77].

Supplementary Information The online version contains supplementary material available at https://doi.org/10.1007/s42114-025-01331-z.

Author contribution These authors contributed equally: Kyeong-Mo Koo, Seung Ju Seo. Y.J. and T.-H.K. supervised the project and conceived the idea. K.-M.K. and S.J.S. contributed equally to this project. K.-M.K. and S.J.S. sourced materials and conducted experiments. K.-M.K. developed the PMGN platform for monitoring direct cardiac reprogramming using the EC method. S.J.S. performed the characterization of cardiomyocytes. K.-M.K. carried out most of the EC detection of cardiomyocytes under Y.J. and T.-H.K. & supervision. S.J.S. and H.Y conducted most of the biological experiments, including immunofluorescence staining, RT-qPCR, OCR evaluation, and calcium transient measurements, supervised by Y.J. and T.-H.K. K.-M.K., S.J.S., and C.-D.K. organized the data. K.-M.K., S.J.S., C.-D.K., Y.J., and T.-H.K. analyzed the data and wrote the manuscript. All authors reviewed the manuscript.

Funding This research was supported by a National Research Foundation of Korea (NRF) grant funded by the Korea government (MSIT) (Grant No. RS-2021-NR061930), by the Korean Fund for Regenerative Medicine funded by the Ministry of Science and ICT, and the Ministry of Health and Welfare (Grant Nos. RS-2022–00070316), and Korean ARPA-H Project through the KHIDI, funded by the Ministry of Health & Welfare (Grant No. RS-2024-00512240). Additionally, this research was supported by a grant of the Korea Health Technology R&D Project through the Korea Health Industry Development Institute (KHIDI), funded by the Ministry of Health & Welfare (Grant No. RS-2024–00405260).

Data availability No datasets were generated or analysed during the current study.

Declarations

Competing interests The authors declare no competing interests.

Open Access This article is licensed under a Creative Commons Attribution-NonCommercial-NoDerivatives 4.0 International License, which permits any non-commercial use, sharing, distribution and reproduction in any medium or format, as long as you give appropriate credit to the original author(s) and the source, provide a link to the Creative Commons licence, and indicate if you modified the licensed material. You do not have permission under this licence to share adapted material derived from this article or parts of it. The images or other third party material in this article are included in the article's Creative Commons licence, unless indicated otherwise in a credit line to the material. If material is not included in the article's Creative Commons licence and your intended use is not permitted by statutory regulation or exceeds the permitted use, you will need to obtain permission directly from the copyright holder. To view a copy of this licence, visit https://creativecommons.org/licenses/by-nc-nd/4.0/.

References

- Mensah GA, Fuster V, Murray CJ, Roth GA (2023) Global burden of cardiovascular diseases and risks, 1990–2022. JACC. 82(25):2350–2473. https://doi.org/10.1016/j.jacc.2023.11.007
- Giudicessi JR, Kullo IJ, Ackerman MJ (2017) Precision cardiovascular medicine: state of genetic testing. Mayo Clinic Proceedings. 92(4):642s–6662. https://doi.org/10.1016/j.mayocp.2017.01.015
- Cahill TJ, Choudhury RP, Riley PR (2017) Heart regeneration and repair after myocardial infarction: translational opportunities for novel therapeutics. Nat. Rev. Drug Discov. 16(10):s699–717. https://doi.org/10.1038/nrd.2017.106
- Wang H, Yang Y, Liu J, Qian L (2021) Direct cell reprogramming: approaches, mechanisms and progress. Nat. Rev. Mol. Cell Biol. 22(6):410–424. https://doi.org/10.1038/s41580-021-00335-z
- Grath A, Dai G (2019) Direct cell reprogramming for tissue engineering and regenerative medicine. J. Biol. Eng. 13(1):14. https://doi.org/10.1186/s13036-019-0144-9
- Sadahiro T, Yamanaka S, Ieda M (2015) Direct cardiac reprogramming: progress and challenges in basic biology and clinical applications. Circ. Res. 116(8):1378–1391. https://doi.org/10.1161/CIRCRESAHA.116.305374
- Wang J, Gu S, Liu F, Chen Z, Xu H, Liu Z, Cheng W, Wu L, Xu T, Chen Z (2022) Reprogramming of fibroblasts into expandable cardiovascular progenitor cells via small molecules in xeno-free conditions. Nat. Biomed. Eng. 6(4):403–420. https://doi.org/10.1038/s41551-022-00865-7
- Fu Y, Huang C, Xu X, Gu H, Ye Y, Jiang C, Qiu Z, Xie X (2015) Direct reprogramming of mouse fibroblasts into cardiomyocytes with chemical cocktails. Cell Res. 25(9):1013–1024. https://doi. org/10.1038/cr.2015.99
- Nam Y-J, Lubczyk C, Bhakta M, Zang T, Fernandez-Perez A, McAnally J, Bassel-Duby R, Olson EN, Munshi NV (2014) Induction of diverse cardiac cell types by reprogramming fibroblasts with cardiac transcription factors. Development. 141(22):4267–4278. https://doi.org/10.1242/dev.114025



- 10. Jin Y, Kim H, Min S, Choi YS, Seo SJ, Jeong E, Kim SK, Lee H-A, Jo S-H, Park J-H (2022) Three-dimensional heart extracellular matrix enhances chemically induced direct cardiac reprogramming. Sci Adv 8(50):eabn5768. https://doi.org/10.1126/sciadv. abn5768
- 11. Min S, Lee H-J, Jin Y, Kim YH, Sung J, Choi H-J, Cho S-W (2020) Biphasic electrical pulse by a micropillar electrode array enhances maturation and drug response of reprogrammed cardiac spheroids. Nano Lett. 20(10):6947-6956. https://doi.org/10.1021/ acs.nanolett.0c01141
- 12. Park G, Yoon BS, Kim YS, Choi S-C, Moon J-H, Kwon S, Hwang J, Yun W, Kim J-H, Park C-Y (2015) Conversion of mouse fibroblasts into cardiomyocyte-like cells using small molecule treatments. Biomaterials. 54:201-212. https://doi.org/10.1016/j.bioma terials.2015.02.029
- 13. Song M, Choi DB, Im JS, Song YN, Kim JH, Lee H, An J, Kim A, Choi H, Kim J-C (2024) Modeling acute myocardial infarction and cardiac fibrosis using human induced pluripotent stem cellderived multi-cellular heart organoids. Cell Death Dis. 15(5):308. https://doi.org/10.1038/s41419-024-06703-9
- 14. Yazawa M, Hsueh B, Jia X, Pasca AM, Bernstein JA, Hallmayer J, Dolmetsch RE (2011) Using induced pluripotent stem cells to investigate cardiac phenotypes in timothy syndrome. Nature. 471(7337):230-234. https://doi.org/10.1038/nature09855
- 15. Blinova K, Dang Q, Millard D, Smith G, Pierson J, Guo L, Brock M, Lu HR, Kraushaar U, Zeng H (2018) International multisite study of human-induced pluripotent stem cell-derived cardiomyocytes for drug proarrhythmic potential assessment. Cell Rep. 24(13):3582–3592. https://doi.org/10.1016/j.celrep.2018.08.079
- 16. Min S, Kim S, Sim W-S, Choi YS, Joo H, Park J-H, Lee S-J, Kim H, Lee MJ, Jeong I (2024) Versatile human cardiac tissues engineered with perfusable heart extracellular microenvironment for biomedical applications. Nat. Commun. 15(1):2564. https:// doi.org/10.1038/s41467-024-46928-y
- 17. Giacomelli E, Meraviglia V, Campostrini G, Cochrane A, Cao X, Van Helden RW, Garcia AK, Mircea M, Kostidis S, Davis RP (2020) Human-ipsc-derived cardiac stromal cells enhance maturation in 3d cardiac microtissues and reveal non-cardiomyocyte contributions to heart disease. Cell Stem Cell 26(6):862-879. e811. https://doi.org/10.1016/j.stem.2020.05.004
- 18. Wang H, Cao N, Spencer CI, Nie B, Ma T, Xu T, Zhang Y, Wang X, Srivastava D, Ding S (2014) Small molecules enable cardiac reprogramming of mouse fibroblasts with a single factor, oct4. Cell Rep. 6(5):951–960. https://doi.org/10.1016/j.celrep.2014.01.
- 19. Zhou Y, Wang L, Liu Z, Alimohamadi S, Yin C, Liu J, Qian L (2017) Comparative gene expression analyses reveal distinct molecular signatures between differentially reprogrammed cardiomyocytes. Cell Rep. 20(13):3014-3024. https://doi.org/10.1016/j. celrep.2017.09.005
- 20. Liras A (2010) Future research and therapeutic applications of human stem cells: general, regulatory, and bioethical aspects. J. Transl. Med. 8:1-15. https://doi.org/10.1186/1479-5876-8-131
- Beheshtizadeh N, Gharibshahian M, Pazhouhnia Z, Rostami M, Zangi AR, Maleki R, Azar HK, Zalouli V, Rajavand H, Farzin A (2022) Commercialization and regulation of regenerative medicine products: promises, advances and challenges. Biomed. Pharmacother. 153:113431. https://doi.org/10.1016/j.biopha.2022.
- 22. Rohani L, Johnson AA, Naghsh P, Rancourt DE, Ulrich H, Holland H (2018) Concise review: molecular cytogenetics and quality control: clinical guardians for pluripotent stem cells. Stem Cells Transl. Med. 7(12):867-875. https://doi.org/10.1002/sctm.
- 23. Koo K-M, Kim C-D, Kim H, Cho Y-W, Suhito I-R, Kim T-H (2023) Extracellularly detectable electrochemical signals of living

- cells originate from metabolic reactions. Adv. Sci. 10(9):2207084. https://doi.org/10.1002/advs.202207084
- 24. Koo K-M, Go Y-H, Kim S-M, Kim C-D, Do JT, Kim T-H, Cha H-J (2023) Label-free and non-destructive identification of naïve and primed embryonic stem cells based on differences in cellular metabolism. Biomaterials. 293:121939. https://doi.org/10.1016/j. biomaterials.2022.121939
- 25. Gaspar JA, Doss MX, Hengstler JG, Cadenas C, Hescheler J, Sachinidis A (2014) Unique metabolic features of stem cells, cardiomyocytes, and their progenitors. Circ. Res. 114(8):1346–1360. https://doi.org/10.1161/CIRCRESAHA.113.302021
- 26. Feyen DA, McKeithan WL, Bruyneel AA, Spiering S, Hörmann L, Ulmer B, Zhang H, Briganti F, Schweizer M, Hegyi B (2020) Metabolic maturation media improve physiological function of human ipsc-derived cardiomyocytes. Cell Rep. 32(3):107925. https://doi.org/10.1016/j.celrep.2020.107925
- Garbern JC, Lee RT (2021) Mitochondria and metabolic transitions in cardiomyocytes: lessons from development for stem cellderived cardiomyocytes. Stem cell res. ther. 12:1–25. https://doi. org/10.1186/s13287-021-02252-6
- 28. Chung S, Dzeja PP, Faustino RS, Perez-Terzic C, Behfar A, Terzic A (2007) Mitochondrial oxidative metabolism is required for the cardiac differentiation of stem cells. Nat. Clin. Pract. Cardiovasc. Med. 4(Suppl 1):S60-S67. https://doi.org/10.1038/ncpcardio0766
- 29. Karbassi E, Fenix A, Marchiano S, Muraoka N, Nakamura K, Yang X, Murry CE (2020) Cardiomyocyte maturation: advances in knowledge and implications for regenerative medicine. Nat. Rev. Cardiol. 17(6):341-359. https://doi.org/10.1038/ s41569-019-0331-x
- 30. Hayat R (2023) Dynamics of metabolism and regulation of epigenetics during cardiomyocytes maturation. Cell Biol. Int. 47(1):30-40. https://doi.org/10.1002/cbin.11931
- 31. Tan SH, Ye L (2018) Maturation of pluripotent stem cell-derived cardiomyocytes: a critical step for drug development and cell therapy. J. Cardiovasc. Transl. Res. 11:375-392. https://doi.org/ 10.1007/s12265-018-9801-5
- Jin Y, Lee JS, Kim J, Min S, Wi S, Yu JH, Chang G-E, Cho A-N, Choi Y, Ahn D-H (2018) Three-dimensional brain-like microenvironments facilitate the direct reprogramming of fibroblasts into therapeutic neurons. Nat. Biomed. Eng. 2(7):522-539. https://doi. org/10.1038/s41551-018-0260-8
- 33. Rovini A, Heslop K, Hunt EG, Morris ME, Fang D, Gooz M, Gerencser AA, Maldonado EN (2021) Quantitative analysis of mitochondrial membrane potential heterogeneity in unsynchronized and synchronized cancer cells. FASEB J. 35(1):e21148. https://doi.org/10.1096/fj.202001693R
- 34. Heslop K, Rovini A, Hunt E, Fang D, Morris M, Christie C, Gooz M, DeHart D, Dang Y, Lemasters J (2020) Jnk activation and translocation to mitochondria mediates mitochondrial dysfunction and cell death induced by vdac opening and sorafenib in hepatocarcinoma cells. Biochem. Pharmacol. 171:113728. https://doi. org/10.1016/j.bcp.2019.113728
- van Meer BJ, Sala L, Tertoolen LGJ, Smith GL, Burton FL, Mummery CL (2018) Quantification of muscle contraction in vitro and in vivo using MUSCLEMOTION software: from stem cellderived cardiomyocytes to zebrafish and human hearts. Curr. Protoc. Hum. Genet. 99:e67. https://doi.org/10.1002/cphg.67
- Bechelany M, Maeder X, Riesterer J, Hankache J, Lerose D, Christiansen S, Michler J, Philippe L (2010) Synthesis mechanisms of organized gold nanoparticles: influence of annealing temperature and atmosphere. Cryst. Growth Des. 10(2):587–596. https://doi.org/10.1021/cg900981q
- Szunerits S, Praig VG, Manesse M, Boukherroub R (2008) Gold island films on indium tin oxide for localized surface plasmon sensing. Nanotechnology. 19(19). https://doi.org/10.1088/0957-4484/19/19/195712



- Suhito IR, Kim JW, Koo KM, Nam SA, Kim YK, Kim TH (2022) In situ detection of kidney organoid generation from stem cells using a simple electrochemical method. Adv. Sci. 9(20):2200074. https://doi.org/10.1002/advs.202200074
- Vega-Naredo I, Loureiro R, Mesquita K, Barbosa I, Tavares L, Branco A, Erickson J, Holy J, Perkins E, Carvalho R (2014) Mitochondrial metabolism directs stemness and differentiation in p19 embryonal carcinoma stem cells. Cell Death Differ. 21(10):1560– 1574. https://doi.org/10.1038/cdd.2014.66
- Spitkovsky D, Sasse P, Kolossov E, Böttinger C, Fleischmann BK, Hescheler J, Wiesner RJ (2004) Activity of complex iii of the mitochondrial electron transport chain is essential for early heart muscle cell differentiation. FASEB J. 18(11):1300–1302. https:// doi.org/10.1096/fj.03-0520fje
- Li X, Wu F, Günther S, Looso M, Kuenne C, Zhang T, Wiesnet M, Klatt S, Zukunft S, Fleming I (2023) Inhibition of fatty acid oxidation enables heart regeneration in adult mice. Nature. 622(7983):619–626. https://doi.org/10.1038/s41586-023-06585-5
- Eaton S, Bartlett K, Quant PA (2001) Carnitine palmitoyl transferase i and the control of β-oxidation in heart mitochondria. Biochem. Biophys. Res. Commun. 285(2):537–539. https://doi.org/10.1006/bbrc.2001.5201
- 43. He L, Kim T, Long Q, Liu J, Wang P, Zhou Y, Ding Y, Prasain J, Wood PA, Yang Q (2012) Carnitine palmitoyltransferase-1b deficiency aggravates pressure overload–induced cardiac hypertrophy caused by lipotoxicity. Circulation. 126(14):1705–1716. https://doi.org/10.1161/CIRCULATIONAHA.111.075978
- 44. Wang X, Zhu X-X, Jiao S-Y, Qi D, Yu B-Q, Xie G-M, Liu Y, Song Y-T, Xu Q, Xu Q-B (2022) Cardiomyocyte peroxisome proliferator-activated receptor α is essential for energy metabolism and extracellular matrix homeostasis during pressure overload-induced cardiac remodeling. Acta Pharmacol. Sin. 43(5):1231–1242. https://doi.org/10.1038/s41401-021-00743-z
- Kersten S (2014) Integrated physiology and systems biology of pparα. Mol. Metab. 3(4):354–371. https://doi.org/10.1016/j.molmet.2014.02.002
- 46. Kaimoto S, Hoshino A, Ariyoshi M, Okawa Y, Tateishi S, Ono K, Uchihashi M, Fukai K, Iwai-Kanai E, Matoba S (2017) Activation of ppar-α in the early stage of heart failure maintained myocardial function and energetics in pressure-overload heart failure. Am. J. Physiol. Heart Circ. Physiol. 312(2):H305–H313. https://doi.org/10.1152/ajpheart.00553.2016
- Kang I, Chu CT, Kaufman BA (2018) The mitochondrial transcription factor tfam in neurodegeneration: emerging evidence and mechanisms. FEBS Lett. 592(5):793–811. https://doi.org/10.1002/1873-3468.12989
- Kunkel GH, Chaturvedi P, Tyagi SC (2016) Mitochondrial pathways to cardiac recovery: Tfam. Heart Fail Rev. 21:499–517. https://doi.org/10.1007/s10741-016-9561-8
- Dinkova-Kostova AT, Abramov AY (2015) The emerging role of nrf2 in mitochondrial function. Free Radic. Biol. Med. 88:179– 188. https://doi.org/10.1016/j.freeradbiomed.2015.04.036
- Chen QM, Maltagliati AJ (2018) Nrf2 at the heart of oxidative stress and cardiac protection. Physiol. Genomics. 50(2):77–97. https://doi.org/10.1152/physiolgenomics.00041.2017
- 51. Ver Heyen M, Heymans S, Antoons G, Reed T, Periasamy M, Awede B, Lebacq J, Vangheluwe P, Dewerchin M, Collen D (2001) Replacement of the muscle-specific sarcoplasmic reticulum Ca²⁺-atpase isoform serca2a by the nonmuscle serca2b homologue causes mild concentric hypertrophy and impairs contraction-relaxation of the heart. Circ Res 89(9):838–846. https://doi.org/10.1161/hh2101.098466
- Fan X, Yao H, Liu X, Shi Q, Lv L, Li P, Wang R, Tang T, Qi K (2020) High-fat diet alters the expression of reference genes in male mice. Front. Nutr. 7:589771. https://doi.org/10.3389/fnut. 2020.589771

- 53. Nicholls C, Li H, Liu JP (2012) GAPDH: a common enzyme with uncommon functions. Clin. Exp. Pharmacol. Physiol. 39(8):674–679. https://doi.org/10.1111/j.1440-1681.2011. 05599.x
- Artero-Castro A, Perez-Alea M, Feliciano A, Leal JA, Genestar M, Castellvi J, Peg V, Cajal SR, LLeonart ME (2015) Disruption of the ribosomal P complex leads to stress-induced autophagy. Autophagy 11(9):1499–1519. https://doi.org/10.1080/15548627. 2015.1063764
- Yilbas AE, Hamilton A, Wang Y, Mach H, Lacroix N, Davis DR, Chen J, Li Q (2014) Activation of gata4 gene expression at the early stage of cardiac specification. Front. Chem. 2:12. https://doi. org/10.3389/fchem.2014.00012
- Zhou P, He A, Pu WT (2012) Regulation of gata4 transcriptional activity in cardiovascular development and disease. Curr Top Dev Biol 100:143–169. https://doi.org/10.1016/B978-0-12-387786-4. 00005-1
- McCulley DJ, Black BL (2012) Transcription factor pathways and congenital heart disease. Curr Top Dev Biol 100:253–277. https:// doi.org/10.1016/B978-0-12-387786-4.00008-7
- King NM, Methawasin M, Nedrud J, Harrell N, Chung CS, Helmes M, Granzier H (2011) Mouse intact cardiac myocyte mechanics: cross-bridge and titin-based stress in unactivated cells. J. Gen. Physiol 137(1):81–91. https://doi.org/10.1085/jgp.20101 0499
- 59. Ginsburg KS, Bers DM (2004) Modulation of excitation–contraction coupling by isoproterenol in cardiomyocytes with controlled SR Ca²⁺ load and Ca²⁺ current trigger. J. Physiol. 556(2):463–480. https://doi.org/10.1113/jphysiol.2003.055384
- Zhuo X-Z, Wu Y, Ni Y-J, Liu J-H, Gong M, Wang X-H, Wei F, Wang T-Z, Yuan Z, Ma A-Q (2013) Isoproterenol instigates cardiomyocyte apoptosis and heart failure via ampk inactivation-mediated endoplasmic reticulum stress. Apoptosis. 18:800–810. https://doi.org/10.1007/s10495-013-0843-5
- Giorgi C, Marchi S, Pinton P (2018) The machineries, regulation and cellular functions of mitochondrial calcium. Nat. Rev. Mol. Cell Biol. 19(11):713–730. https://doi.org/10.1038/s41580-018-0052-8
- Duchen MR (2000) Mitochondria and calcium: from cell signalling to cell death. J. Physiol. 529(1):57–68. https://doi.org/10. 1111/j.1469-7793.2000.00057.x
- Rossi A, Pizzo P, Filadi R (2019) Calcium, mitochondria and cell metabolism: a functional triangle in bioenergetics. Biochim Biophys Acta Mol Cell Res 1866(7):1068–1078. https://doi.org/ 10.1016/j.bbamcr.2018.10.016
- He J-Q, Ma Y, Lee Y, Thomson JA, Kamp TJ (2003) Human embryonic stem cells develop into multiple types of cardiac myocytes: action potential characterization. Circ. Res. 93(1):32–39. https://doi.org/10.1161/01.RES.0000080317.92718.99
- Linders AN, Dias IB, López Fernández T, Tocchetti CG, Bomer N, Van der Meer P (2024) A review of the pathophysiological mechanisms of doxorubicin-induced cardiotoxicity and aging. npj Aging. 10(1):9 https://doi.org/10.1038/s41514-024-00135-7
- Burridge PW, Li YF, Matsa E, Wu H, Ong S-G, Sharma A, Holmström A, Chang AC, Coronado MJ, Ebert AD (2016) Human induced pluripotent stem cell–derived cardiomyocytes recapitulate the predilection of breast cancer patients to doxorubicin-induced cardiotoxicity. Nat. Med. 22(5):547–556. https://doi.org/10.1038/nm.4087
- Rawat PS, Jaiswal A, Khurana A, Bhatti JS, Navik U (2021) Doxorubicin-induced cardiotoxicity: an update on the molecular mechanism and novel therapeutic strategies for effective management. Biomed. Pharmacother. 139:111708. https://doi.org/10. 1016/j.biopha.2021.111708
- Nabati M, Parsaee H (2022) Potential cardiotoxic effects of remdesivir on cardiovascular system: a literature review.



- Cardiovasc. Toxicol. 22(3):268–272. https://doi.org/10.1007/s12012-021-09703-9
- Choi SW, Shin JS, Park S-J, Jung E, Park Y-G, Lee J, Kim SJ, Park H-J, Lee J-H, Park S-M (2020) Antiviral activity and safety of remdesivir against SARS-CoV-2 infection in human pluripotent stem cell-derived cardiomyocytes. Antiviral Res. 184:104955. https://doi.org/10.1016/j.antiviral.2020.104955
- He H, Tao H, Xiong H, Duan SZ, McGowan FX Jr, Mortensen RM, Balschi JA (2014) Rosiglitazone causes cardiotoxicity via peroxisome proliferator-activated receptor γ-independent mitochondrial oxidative stress in mouse hearts. Toxicol. Sci. 138(2):468–481. https://doi.org/10.1093/toxsci/kfu015
- Nathan DM (2007) Rosiglitazone and cardiotoxicity—weighing the evidence. N Engl J Med 357(1):64–66. https://doi.org/10. 1056/NEJMe078117
- AlAsmari AF, Ali N, AlAsmari F, AlAnazi WA, AlShammari MA, Al-Harbi NO, Alhoshani A, Sobeai HMA, AlSwayyed M, AlAnazi MM (2020) Liraglutide attenuates gefitinib-induced cardiotoxicity and promotes cardioprotection through the regulation of MAPK/NF-κB signaling pathways. Saudi Pharm. J. 28(4):509–518. https://doi.org/10.1016/j.jsps.2020.03.002
- Abbas NA, Kabil SL (2017) Liraglutide ameliorates cardiotoxicity induced by doxorubicin in rats through the Akt/GSK-3β signaling pathway. Naunyn Schmiedebergs Arch Pharmacol. 390:1145– 1153. https://doi.org/10.1007/s00210-017-1414-z

- Goldring CE, Duffy PA, Benvenisty N, Andrews PW, Ben-David U, Eakins R, French N, Hanley NA, Kelly L, Kitteringham NR (2011) Assessing the safety of stem cell therapeutics. Cell Stem Cell. 8(6):618–628. https://doi.org/10.1016/j.stem.2011.05.012
- Lovell-Badge R, Anthony E, Barker RA, Bubela T, Brivanlou AH, Carpenter M, Charo RA, Clark A, Clayton E, Cong Y (2021) ISSCR guidelines for stem cell research and clinical translation: the 2021 update. Stem Cell Rep. 16(6):1398–1408. https://doi.org/ 10.1016/j.stemcr.2021.05.012
- Han S, Cruz SH, Park S, Shin S-R (2023) Nano-biomaterials and advanced fabrication techniques for engineering skeletal muscle tissue constructs in regenerative medicine. Nano Converg. 10(1):48. https://doi.org/10.1186/s40580-023-00398-y
- Kim H, Koo K-M, Kim C-D, Byun M-J, Park C-G, Son H, Kim H-R, Kim T-H (2024) Simple and cost-effective generation of 3D cell sheets and spheroids using curvature-controlled paraffin wax substrates. Nano Converg. 11(1):44. https://doi.org/10.1186/ s40580-024-00451-4

Publisher's Note Springer Nature remains neutral with regard to jurisdictional claims in published maps and institutional affiliations.

